ILLINOIS INSTITUTE OF TECHNOLOGY
CHICAGO

Type: Final Technical Report

Period: October 1, 1992 through March 30, 1995

Grant Number: F49620-93-0157

HYSTERESIS AND ACOUSTIC EMISSION AS NON-DESTRUCTIVE MEASURES OF THE FATIGUE PROCESS IN METALS

19950627 004

S.A. Guralnick
Principal Investigator

T. Erber
Co-Principal Investigator

TABLE OF CONTENTS

Page

CHAPTER I

INTRODUCTION

Metal fatigue is a result of a cumulative damage process due to repeated cyclic loading which causes premature and unpredictable failure. It is a complicated metallurgical process at the microscopic level which is difficult to accurately explain or model. Despite the complexities, fatigue analysis methods have been developed and are being developed to facilitate fatigue damage assessment and the prediction of fatigue life. This research project is concerned with the behavior of metals subjected to cyclic loading carried to failure. The purpose of this investigation is to develop a relationship between hysteresis loss, hysteresis loop drift, strain amplitudes and the number of cycles to failure; and to correlate this phenomenological description of the fatigue process with mesoscopic observables such as acoustic emission and stress-induced magnetization.

Accesion For		
NTIS CRA&I	☑	
DTIC TAB	☐	
Unannounced	☐	
Justification		
By		
Distribution /		
Availability Codes		
Dist	Avail and / or Special	
A-1		

CHAPTER II

SUMMARY OF PREVIOUS RESEARCH

Modern Research Work

Earlier fatigue strength prediction methods, mainly based on stress controlled experiments, were very important from a design standpoint because the stress-cycles to falure diagrams of Wöhler were used to estimate a safe alternating stress level for a given material. The work of Gerber, Launhardt, Weyrauch, Goodman and Johnson helped to determine design criteria for varying stress ranges and amplitudes. However, these methods required a large number of experiments to estimate the endurance limit of a material. Hence, strain controlled experiments using strain as the independent variable became more popular. This was desirable because the instantaneous cross sectional area is difficult to determine, which makes determination of true stress difficult.

Also, separating the total strain into elastic and plastic components by subtracting the elastic component, σ/E, from the total strain became common practice. Figure 2.1 shows a typical hysteresis loop with elastic and plastic components. This division is based on the belief that only the plastic strain component inflicts fatigue damage. Halford (1963) and Mitchell (1978) describe simple procedures for determining the strain hardening exponent, n, true fracture strength, σ_f, true fracture ductility, ϵ_f, and the strength coefficient, K, from monotonic tensile stress-strain experiments. The equation shown below is an attempt to describe a material's monotonic behavior.

$$\epsilon_t = \epsilon_e + \epsilon_p = \frac{\sigma}{E} + \left(\frac{\sigma}{K}\right)^{\frac{1}{n}} \qquad (2.2)$$

where, E = Young's modulus of elasticity, and K = the strength coefficient, σ_f/ϵ_f^n. Similarly, an equation for the cyclic stress-strain curve is presented below:

$$\epsilon_t = \epsilon_e + \epsilon_p' = \frac{\sigma}{E} + \left(\frac{\sigma}{K'}\right)^{\frac{1}{n'}} \qquad (2.3)$$

where, K' and n' are the cyclic stress-strain parameters. The cyclic stress-strain curve can be obtained by plotting different stabilized hysteresis loops from experiments cycled at different strains amplitudes on the same diagram and then connecting the tips of these loops. The locus of these loop tips forms the cyclic stress strain curve. A typical cyclic stress-strain curve is shown in Figure 2.2. The parameters for the cyclic stress-strain diagram are shown with prime symbol.
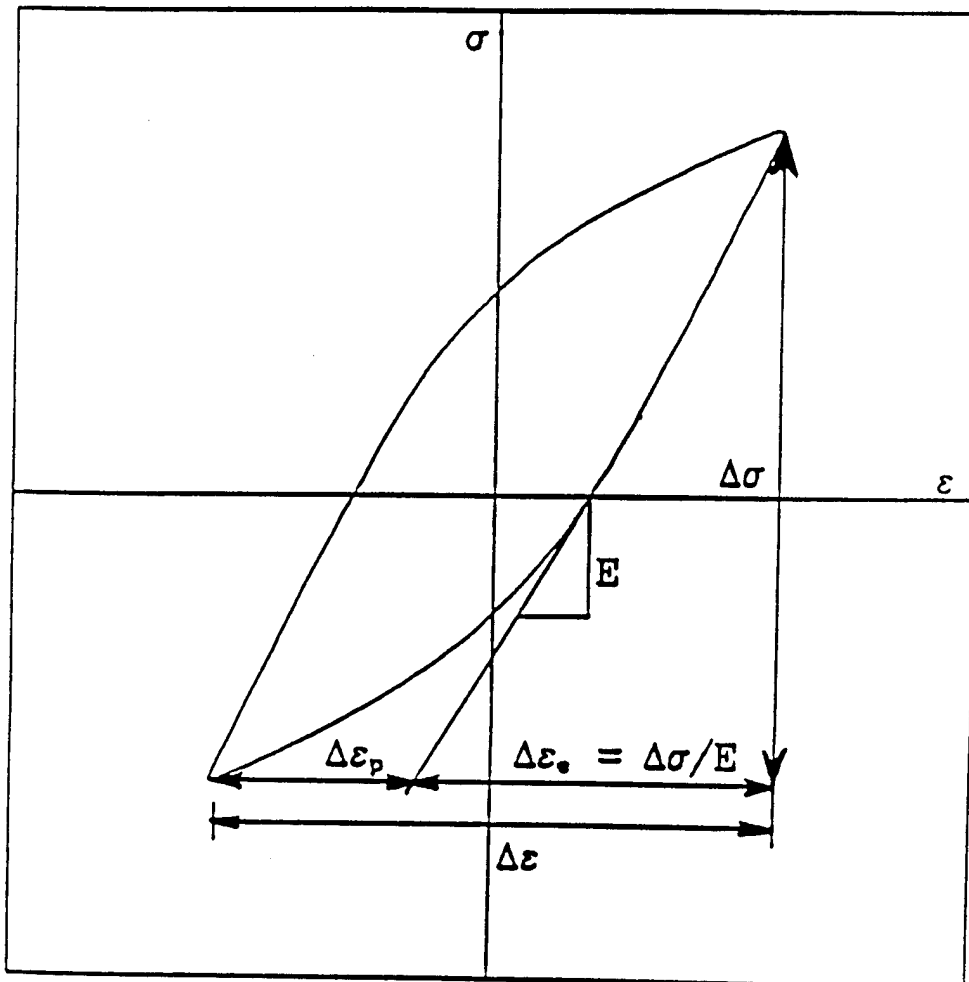
Figure 2.1. Elastic and Plastic Components of a Typical Hysteresis Loop

<u>Energy Methods</u>

This approach is based on the principle of conservation of energy which states that energy can neither be created nor destroyed but can be converted from one form to another or can be transferred from one system to another. The investigation reported herein is based on this approach.

The energy approach involves computation of areas of stress-strain or hysteresis loops. The areas of hysteresis loops have units of kip-in/in^3 which are units of strain energy density. The hysteresis loop area has also been used to define material toughness. Feltner and Morrow (1961) and Halford (1966) felt that it was only the plastic strain energy component that contributed to accumulation of fatigue damage. Feltner and Morrow (1961) define the plastic strain energy per cycle as:

$$\Delta W = 2 \int_0^{\Delta \epsilon_p} \sigma \, d\epsilon_p \tag{2.4}$$

where, ΔW = the plastic strain energy dissipated in one cycle, $\Delta \epsilon_p$ = the total true plastic strain range, and σ = the true instantaneous stress. If the plastic strain energy component per cycle is assumed to be a constant, the total plastic strain energy to failure, or in other words, the fatigue toughness, is given by:

$$W_p = N_f \Delta W = 2N \int_0^{\Delta \epsilon_p} \sigma \, d\epsilon_p \tag{2.5}$$
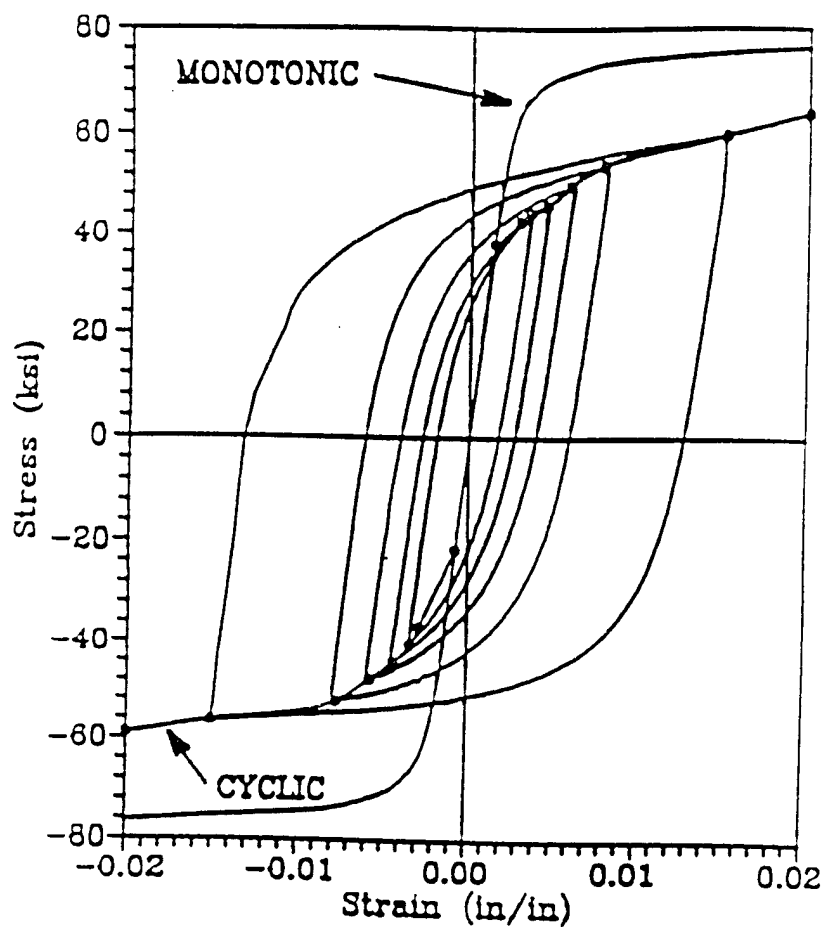
Figure 2.2. Monotonic and Cyclic Stress-Strain Curves

where, W_p = the total plastic strain energy at failure, and N_f = the number of cycles to failure.

This equation, when combined with stress-life equation, has also been given by:

$$\log_{10}\sigma_a = k - (\frac{n}{1+n})\log_{10}N_f \qquad (2.6)$$

where, n = the strain hardening exponent, N_f = the number of cycles to failure, and k = the constant determined from total plastic strain energy to failure. This equation has been found to be reasonably accurate for predicting stress versus number of cycles to failure for intermediate cycle ranges. However, this method is not very accurate near the endurance limit.

Damage Accumulation

Miner (1945) proposed a law which explains the cumulation of damage under cyclic loading. The linear form of Miner's law of cumulative damage is:

$$\sum_{i=1}^{k} \frac{n_i}{N_i} = 1 \qquad (2.7)$$

where, N_i = the number of cycles to failure at the ith stress amplitude, n_i = the actual number of cycles at the ith stress amplitude, and k = the total number of different stress amplitudes. Failure occurs when the sum of the k ratios is equal to 1. This equation assumes a linear variation of the ratio of energy per cycle to total energy to failure. Feltner and Morrow (1961) and Martin (1961) suggested that the total energy required to fracture a specimen under monotonic tension is equal to the amount of damaging energy required to cause

failure in fatigue. Halford (1966) compared the thermal energy required to melt iron with the total energy accumulated over a fatigue life of 500,000 cycles. He explained that the equivalent thermal energy lost over 500,000 cycles is more than nine times the energy required to melt the steel. Martin (1961) concluded that 'total hysteresis energy dissipated cannot be equated to fatigue damage.'

The Fatigue Model

Guralnick (1975) proposed this model which utilizes an analogy between the incremental collapse of structures and the fatigue failure of metals. The plastic collapse, shakedown, and incremental collapse of structures has been investigated by many researchers; for example, Symonds (1952), Neal (1956), Popov and McCarthy (1960), Cohn, Ghosh, and Parimi, (1972), Guralnick (1973), Popov and Bertero (1973), Popov and Peterson (1978), Guralnick, Singh, and Erber (1984), and Guralnick, Erber, Soudan, and He (1988). The fatigue model previously proposed by Guralnick (1975) and presented herein shows the direct analogy between progressive failure of structures by incremental collapse, and the fatigue failure of metals under cyclic loading.

As a structure is loaded to a critical load, plastic hinges form at specific locations in the structure based on the geometry of the structure and the geometry of loading. The formation of a plastic hinge is analogous to the formation of slip bands in a metal. This model considers these slip bands as regions of microplasticity. The location and number of the plastic hinges, if it results in a certain pattern, can result in a collapse mechanism which causes the failure of the structure. The number of plastic hinges required to form a collapse mechanism is:

$$N_c = s^\circ + 1 \qquad\qquad (2.8)$$

where, N_c=the number of plastic hinges at collapse, and s°=the degree of statical indeterminacy of the structure. It is possible for more than N_c plastic hinges to form in a structure during a particular load cycle. However, collapse occurs if and only if the N_c plastic hinges organize into a specific configuration called collapse mechanism. The collapse mechanism for a structure loaded monotonically to failure is not necessarily the same as that which leads to incremental collapse under under cyclic loading. This model suggests that failure in a metal occurs when a critical number of microplastic regions organize themselves into a particular configuration. Because of the inherent complexity of material composition, an infinite number of combinations of microplastic configurations are possible. Hence, the actual positioning and/or physical location of these microplastic zones is not known. Figure 2.3 shows a micrograph showing slip bands of the surface of a mild steel specimen just after yield has been reached by Nadai (1931). This figure displays an organization of the microplastic regions. Use of a finite element mesh to model a continuous solid is an example of this type of approach. The finite element mesh resembles the structure of a rigid frame building. Many ferrous metals are composed of crystals which form grain structures. These grain structures are regular throughout a solid and possess irregularities along grain boundaries. Guralnick (1973), Guralnick (1975), Guralnick, Singh, and Erber (1984), and Guralnick, Erber, Stefanis, and Soudan (1986) have shown that the failure of structures under cyclic loading can be fully described by means of energy methods.
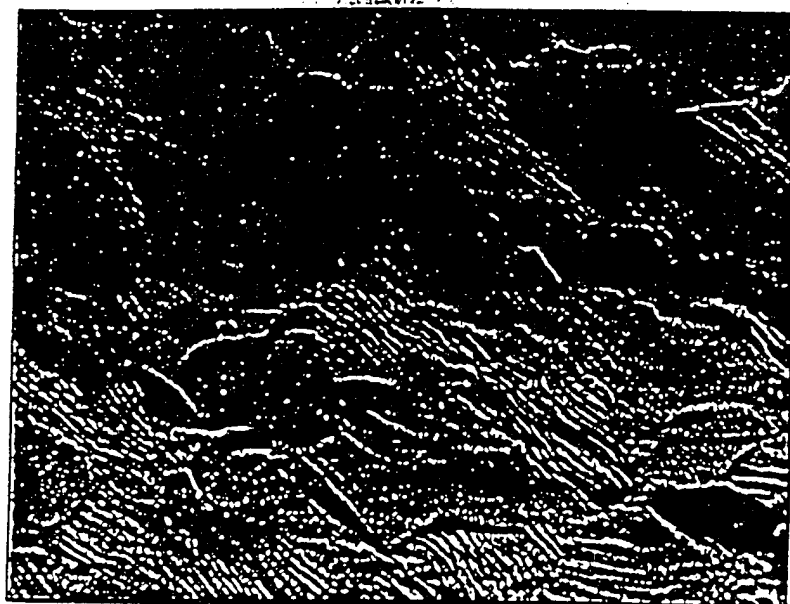
Figure 2.3. Micrograph of a Steel Surface After Yielding Showing Slipbands

If the total irrecoverable energy, absorbed by a structure is unbounded, then the structure must ultimately fail. Or, if the hysteresis energy loss per cycle becomes a constant, then the total hysteresis loss must also become infinite as the number of cycles grows large without bound. Since this is impossible, the structure must fail under a finite number of cycles. However, if the hysteresis loss per cycle becomes zero as the number of cycles increases to infinity, then the total hysteresis loss is finite and the structure will not fail. This is given in a mathematical form by:

$$U_T(W_{max}, n) = \sum_{i=1}^{n} U_i(W_{max}) \qquad (2.9)$$

where,

$$U_i(W_{max}) = \sum_{j=1}^{J(i)} \sum_{k=1}^{K(i)} \Delta U_{ijk}(W_{max}) \qquad (2.10)$$

where, $\Delta U_{ijk} (W_{max}) =$ the energy absorbed by the kth plastic hinge of the jth program step of the ith load cycle, $U_i(W_{max}) =$ the total energy absorbed in the ith load cycle, and $U_T(W_{max}, n) =$ the total energy absorbed by the structure over a lifetime of n load cycles. The amount of energy absorbed by a structure is computed by summing the products of the magnitudes of the fully plastic moments and the corresponding rotations of the members at the positions of the respective plastic hinges. This computation yields the actual quantity of irrecoverable energy imparted to the structure at specific locations. Guralnick (1973) was able to replicate load values corresponding to W_a, the load at which a structure will fail due to alternating plasticity, W_s, the shakedown load below which failure will not occur, and W_c, the plastic collapse load by means of the energy method described above.
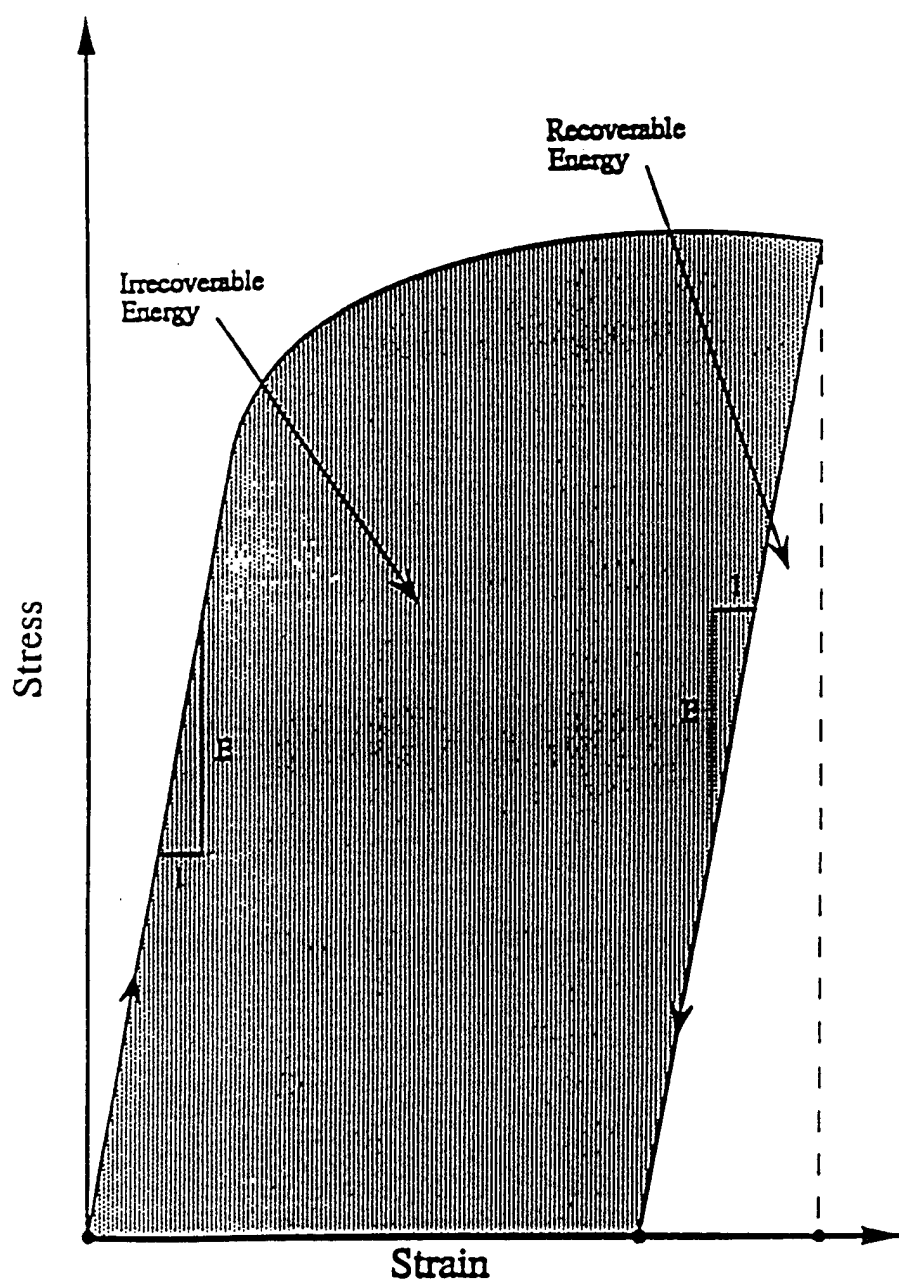
Figure 2.4. Irrecoverable and Recoverable Energy

CHAPTER III

EXPERIMENTAL TECHNIQUES

Material Properties

The material used in this research is unannealed steel (cold finished) conforming to AISI 1018. The choice of material is based on its wide applications in structural steel members. A typical stress-strain curve to failure for this material is shown in Figure 3.1. This particular stress-strain diagram was obtained by using an electronically-controlled servohydraulic cyclic testing machine which is described later on in this chapter. It may be observed from this diagram that the material is of the gradual yielding type because it does not exhibit a sharply-defined yield point. Therefore, a so-called yield point may be determined by the 0.2% offset method. The mechanical properties of ten specimens of the material measured in axial tension tests are listed in Table 3.2. These values are consistent with those described in The American Society for Metals Handbook (II - 1986). The chemical composition of the material is shown in Table 3.1 which also conforms to corresponding information in The American Society for Metals Handbook (II - 1986).

The material, in the form of 3/4" diameter round bars, was used to prepare all of the axial load fatigue test specimens. In all, thirty six axial fatigue test specimens, conforming to the dimensions shown in Figure 3.2, were used. The specimens were machined according to ASTM standard tolerances using a high speed lathe equipped with a carbide cutting tool. Finally, the specimens were hand polished to remove those surface blemishes which were visible under a 2X magnifier.

Table 3.1. Chemical Composition of AISI 1018 Unannealed Steel

Element	Percentile Weight
Manganese	0.75
Carbon	0.16
Copper	0.06
Chromium	0.04
Nickel	0.04
Silicon	0.04
Molybdenum	0.02
Sulfur	0.016
Phosphorous	0.012

Test Setup

An MTS 810 Material Testing System was used for all of the fatigue tests. This is a closed loop, servo valve controlled high performance test system consisting of the components shown in Figure 3.3. All of the tests were set up to run under strain control. The test system used has a force capacity of $\pm$ 22 kips, which is controlled and monitored by means of a load cell sensor. A special extensometer, made from a 3 in $\times$ 0.5 in strip of 10 gauge steel, was used for strain measurement. Electric resistance strain gauges in a standard Wheatstone bridge circuit were used to fabricate this special extensometer. The extensometer was calibrated with a mechanical micrometer and a voltmeter for a maximum full scale strain of $\pm$ 0.022 in/in or $\pm$ 2.2 %.

Table 3.2. Axial Tensile Properties of AISI 1018 Unannealed Steel

Specimen Number	Diameter (inches)	Gage Length (inches)	Yield Strength (psi)	Ultimate Strength (psi)	Elongation (%)	Reduction in Area (%)
AX121	0.505	2.000	70,150	77,090	18.05	61.83
AX122	0.506	2.000	69,620	77,280	18.40	61.74
AX221	0.506	2.000	71,610	78,270	17.95	61.25
AX222	0.506	2.000	72,360	78,570	18.65	61.49
AX321	0.506	2.000	72,110	79,370	17.20	58.75
AX322	0.506	2.000	71,610	79,370	17.25	58.49
AX421	0.506	2.000	67,880	74,490	19.10	61.98
AX422	0.506	2.000	68,130	74,390	18.70	62.47
AX521	0.506	2.000	72,110	79,170	18.40	61.00
AX522	0.506	2.000	72,110	79,170	18.30	61.49
Average	0.506	2.000	70,769	77,717	18.20	61.05
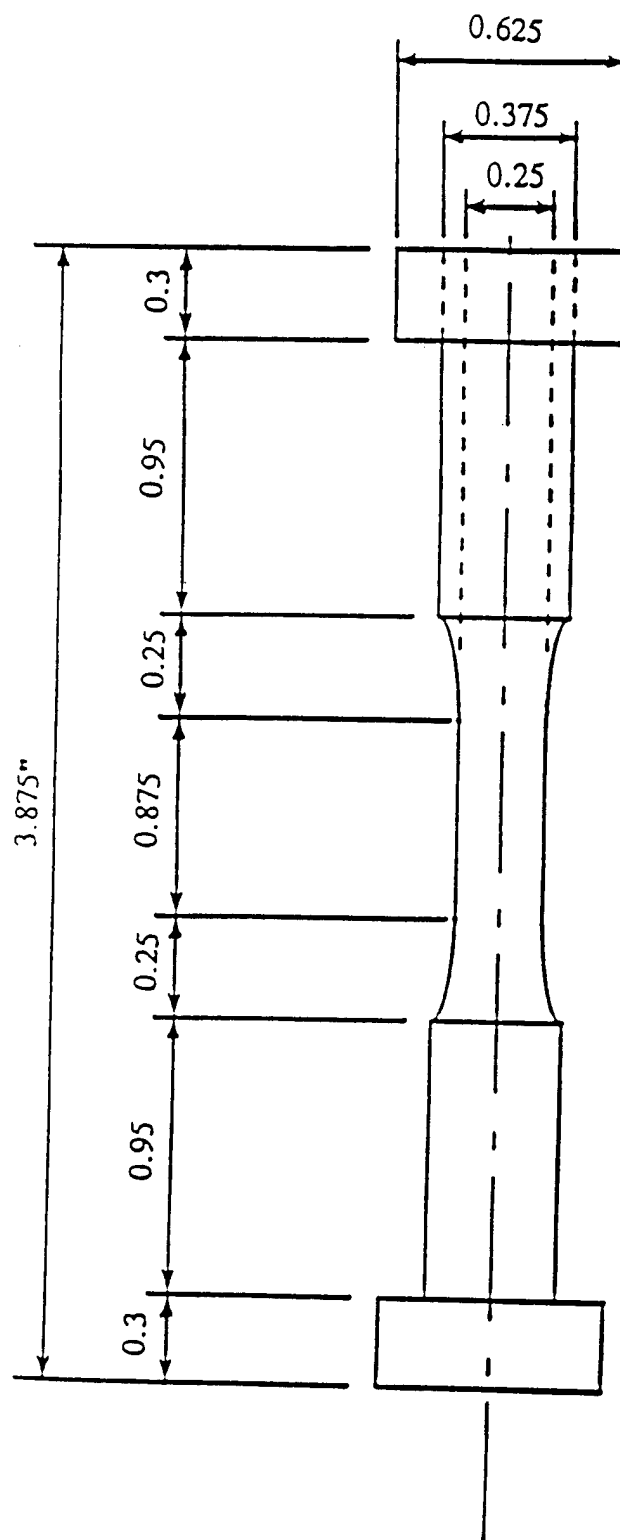
Figure 3.2. Axial Fatigue Test Specimen

458.20 MicroConsole™


Load Unit

Hydraulic Power Supply
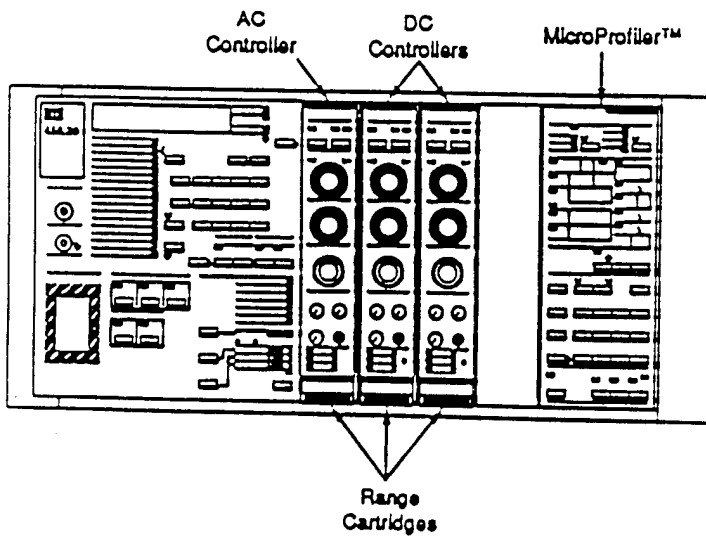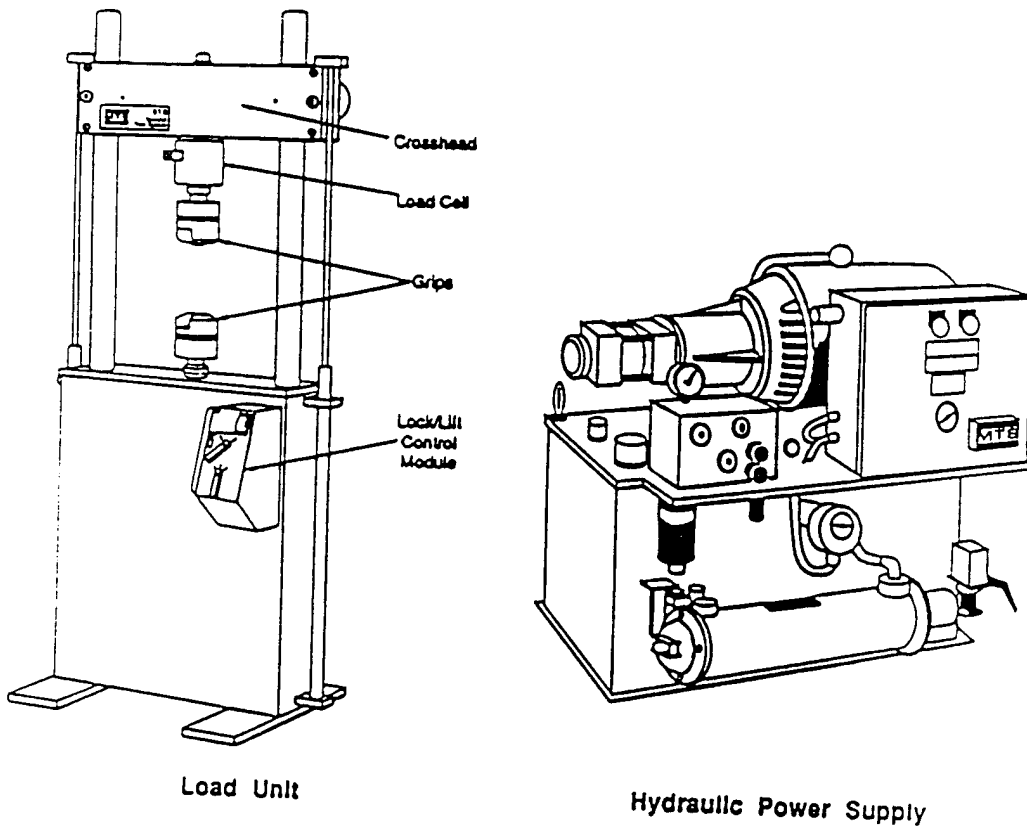
Figure 3.3. MTS Material Testing System Series 810

The functional diagram of the MTS 810 testing system is shown in Figure 3.4. In this closed loop hydraulic testing system, program commands are generated by means of a 'MicroProfiler', which can be set up to produce triangular, rectangular or sine waves. Only triangular waveforms were used in this investigation. The signal from the MicrpProfiler is supplied to a servovalve. This servovalve in turn uses the control signal from the MTS Micro console to regulate the movement of the hydraulic force actuator. The control signal is created by comparing the program command signal (corresponding to the desired actuator position) with the feedback signal from a transducer (corresponding to the actual actuator position). When the program command signal differs from the feedback signal, the voltage difference between the two (i.e. the DC error) is converted into servovalve movement which supplies hydraulic fluid to the actuator until the desired actuator position is achieved. The ability of the servovalve to convert changes in voltage into precise changes in the rate and direction of hydraulic fluid flow makes it suitable for cyclic fatigue tests.

The problems associated with aligning the specimen with the axis of loading were minimized by using special grips obtained from the MTS corporation. The grip and specimen assembly is shown in Figure 3.5. Also, by using MTS spiral washers at both ends of the grip assembly, the risk of backlash or back and forth slip was minimized. Mounting of specimens was done with great care. As a first step, the load frame cross head was brought down to a suitable working position. Specimens were mounted on the top grip, which is connected to the load cell or sensor, and then the actuator piston was brought up to slide the specimens into the bottom grip. A feeler gauge was used, while tightening the bolts through the grip cap into the grip base, to measure the gap between grip base and grip
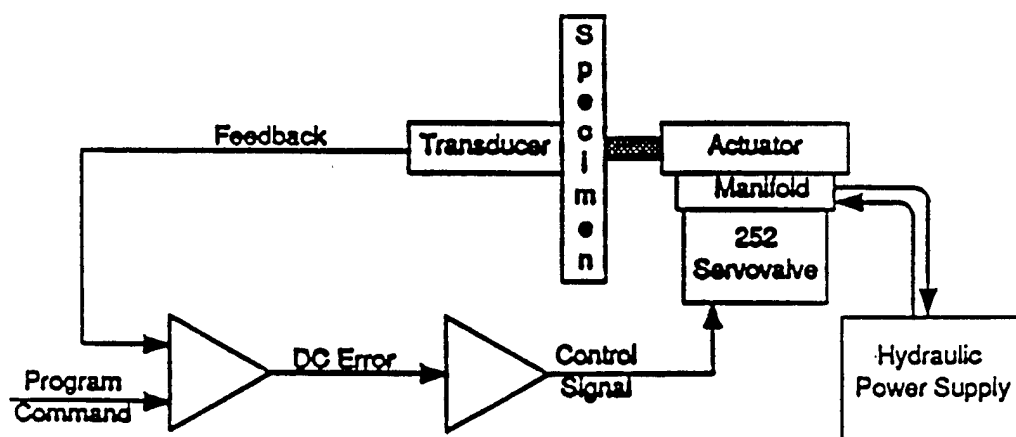
Figure 3.4. Closed Loop Servovalve Controlled System (Functional Diagram)
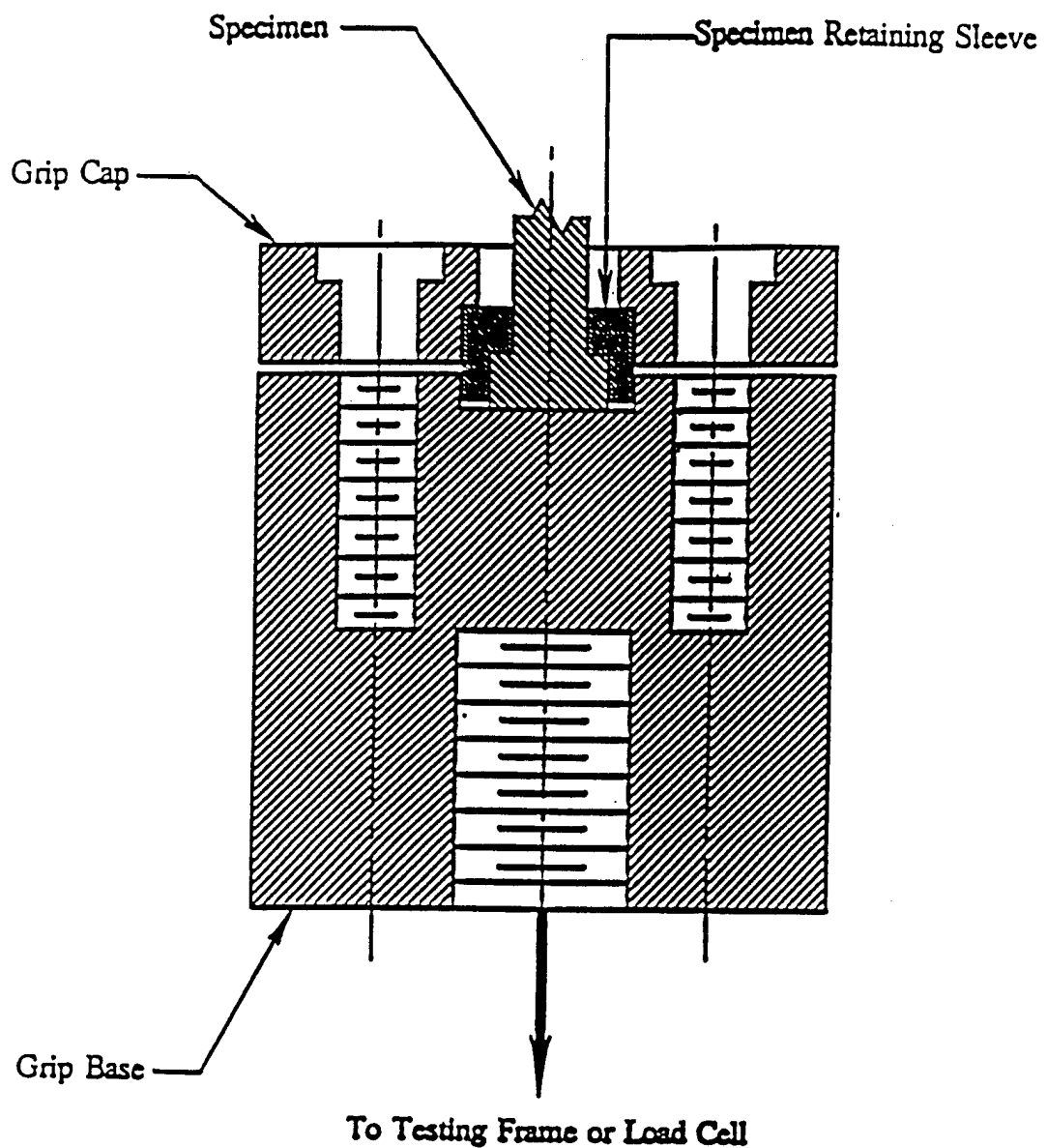
Figure 3.5. Cross Sectional View of Grip and Specimen

cap to ensure an even pressure distribution over the specimen's top and bottom surfaces which were in contact with the grip base.The extensometer was attached to the specimen by using wrap-around springs. Small tape strips were put on the specimen where the extensometer jaws were in contact with the specimen to minimize slippage. The extensometer was connected to the MTS MicroConsole controller.

The strain-controlled loading program, based on the load waveform desired, was created and the MicroProfiler was programmed accordingly. In all cases, the loading program conformed to a triangular waveform. The ordinate of the strain versus time wave, expressed as a percentage of full scale strain, represented the maximum strain level to be achieved. The slope of the wave, expressed as percent per second, represented the rate at which this strain level was to be reached. Test durations of 10 seconds and 2 seconds were used. Typical waveforms and corresponding hysteresis loops for one-sided and two-sided tests are shown in Figure 3.6 and Figure 3.7.

Data Acquisition

The data acquisition was accomplished by using an 80386 desk-top computer system equipped with a DT2801 Data Translation coprocessor board and Labtech NoteBook data acquisition software. The signal from the MTS testing system controller is a voltage output. It is processed by means of the coprocessor board and converted into a digital signal which then becomes an input to the NoteBook data collection software. In a typical test run, stress and strain data records were obtained with a sampling rate of 100 samples per cycle. This rate was found to be satisfactory for computing the area of hysteresis loops without compromising accuracy and without overloading the data acquisition system.

Computation of Hysteresis Loop Area

The raw data obtained from the MTS testing system was further processed to compute the hysteresis loop area. The process of computing the hysteresis loop area is based on the trapezoidal rule which is given by the following equation,

$$\Delta U_i(\epsilon) = \oint \sigma \, d\epsilon \cong \sum_{i=1}^{nd} \frac{1}{2}(\sigma_i + \sigma_{i-1})(\epsilon_i - \epsilon_{i-1}) \qquad (3.1)$$

where,

$\Delta U_i(\epsilon)$ = Hysteresis loop area increment for the ith data point in a particular test cycle,

nd = Number of data points in a particular test cycle,

σ_i, σ_{i-1} = Stress values corresponding to respective data points,

$\epsilon_i, \epsilon_{i-1}$ = Strain values corresponding to respective data points.

The programs developed using the MicroSoft version 5.0 FORTRAN compiler to compute hysteresis loop area for one-sided tests and two-sided tests are listed in Appendix B and in Appendix C, respectively.
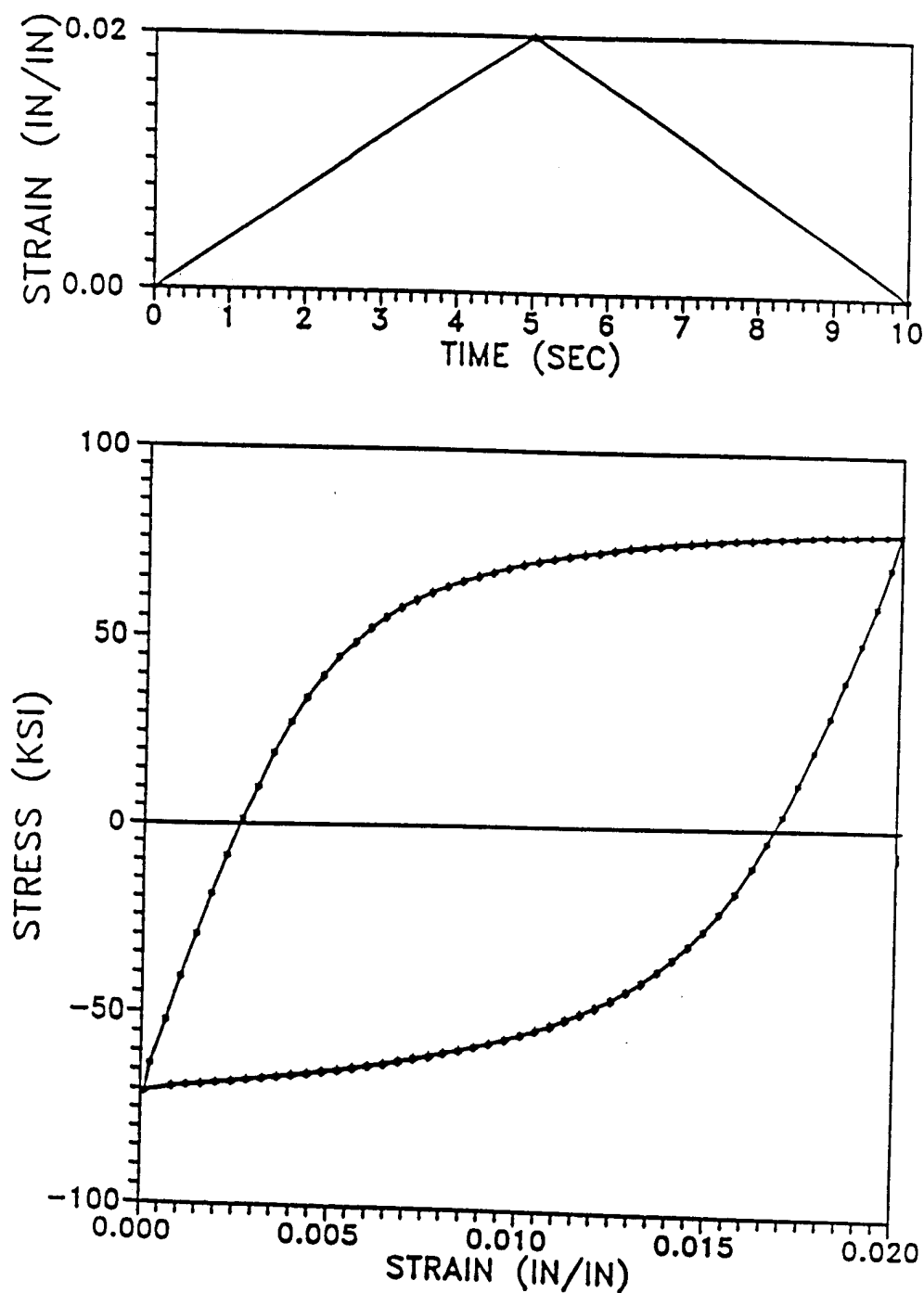
Figure 3.6. Typical Hysteresis Loop and Loading Waveform for One-sided Tests
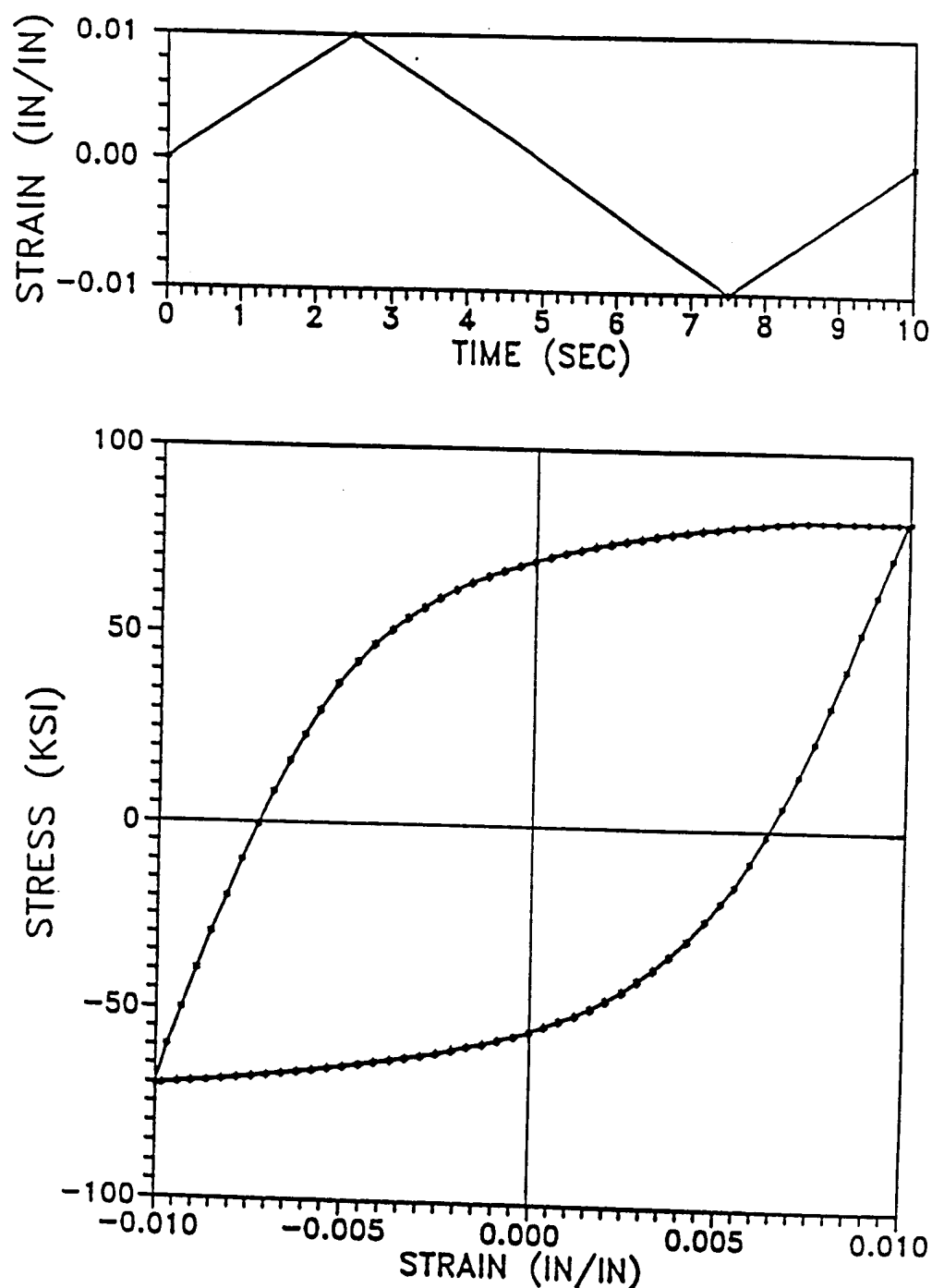
Figure 3.7. Typical Hysteresis Loop and Loading Waveform for Two-Sided Tests

Computation of Hysteresis Loop Drift

The second part of the analysis of the hysteresis loops or stress-strain data consists of computing the amount by which the hysteresis loops drift in the stress-strain plane. As mentioned earlier, all the experiments conducted under strain control, that is, the strain level was kept constant and the response of the specimen was measured in terms of load or engineering stress. Hence, the loop drift was computed in terms of stress values or with respect to the stress axis.

Figure 3.8 demonstrates the typical hysteresis loop drift. This figure shows the drift of loops magnified. The first step in developing this method of analysis was based on computing the drift for each data point on loop i with respect to loop i+1 and then summing the absolute values of drifts to obtain the amount of loopdrift. This process was continued until the number of cycles to failure reached N_f. The following equation is a mathematical definition of this method:

$$DRIFT = \sum_{n=1}^{nd} |\sigma_i - \sigma_{i+1}|$$ (3.2)

where, σ_i and σ_{i+1} are the stresses in ksi for the nth data point in loop i and i+1, respectively and the nth data point is at approximately same strain level in loops i and i+1. The value nd is the number of data points in a particular cycle.

This method of analysis was complicated by certain experimental limitations. The waveform generator of the MTS testing machine and the 80386 computer used to acquire
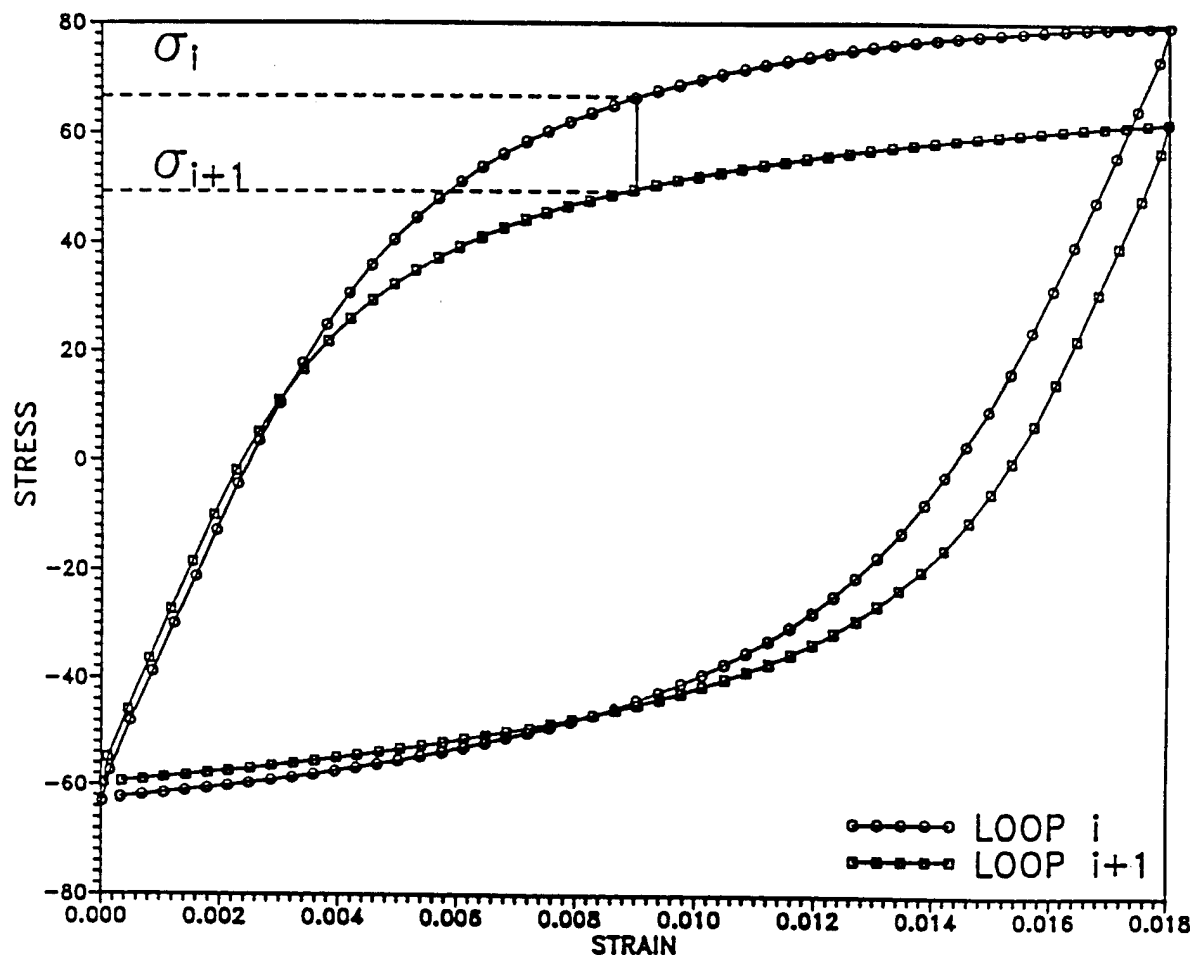
Figure 3.8. Typical Hysteresis Loop Drift

hysteresis data use two physically different clocks. Hence, the data file has a variation in the number of data points recorded in every cycle. The number of data points recorded in each cycle varies between 98 and 100. This makes it impossible to have an one-to-one correspondence between data points from loop to loop which makes it impossible to compute the drift by means of Equation 3.2.

A compromise was made to simplify the analysis. Instead of using all the data points to compute loop drift, only two well defined points, namely, maximum and minimum points were used. Because only two points were used, the effect of change in shape, that is, the width of the loops is not reflected in the computed drift values. However, the values computed in this way were considered to be useful in indicating significant trends. The following formula expresses the mathematical definition of this two-point method.

$$DRIFT = \left|\sigma_{i(\text{max})} - \sigma_{i+1(\text{max})}\right| + \left|\sigma_{i(\text{min})} - \sigma_{i+1(\text{min})}\right| \qquad (3.3)$$

where, $\sigma_{i(\text{max})}$ and $\sigma_{i+1(\text{max})}$ are the maximum stress values for loop i and i+1, respectively, and $\sigma_{i(\text{min})}$ and $\sigma_{i+1(\text{min})}$ are the minimum stress values for loop i and i+1, respectively.

A computer program was developed, using the MicroSoft version 5.0 FORTRAN compiler, to extract maximum and minimum points of hysteresis loops and to compute hysteresis loop drift for one-sided and two-sided experiments. This program is listed in Appendix D.

CHAPTER IV

EXPERIMENTAL RESULTS

The experimental results contained herein are divided into two parts. The first part presents the hysteresis loss measurement results. The second part presents hysteresis loop drift measurement results. Each part is further divided into three parts, that is, results from one-sided experiments, results from two-sided experiments and a combination of results from both the one-sided and two-sided experiments.

Figure 4.1 shows the difference between the one-sided and two-sided experiments conducted at the same strain range. The one-sided hysteresis loop has nonzero mean strain whereas the two-sided hysteresis loop has zero mean strain. Despite the inherent difference between these two types of experiments, it was found that data acquired from both types of experiments are compatible with one another. Or, in other words, the material fails in fatigue in much the same manner in both types of experiments.

Hysteresis Loss Results

The hysteresis loss results were acquired from a program written using Microsoft FORTRAN 5.0 compiler to compute the hysteresis loop area. Figure 4.2 shows a typical graph of hysteresis loss per cycle versus number of cycles. The program also computes cumulative hysteresis loss at every cycle. Figure 4.3 shows a typical graph of cumulative hysteresis loss versus number of cycles. The average hysteresis loss per cycle was computed by dividing cumulative total hysteresis loss by the number of cycles to failure.
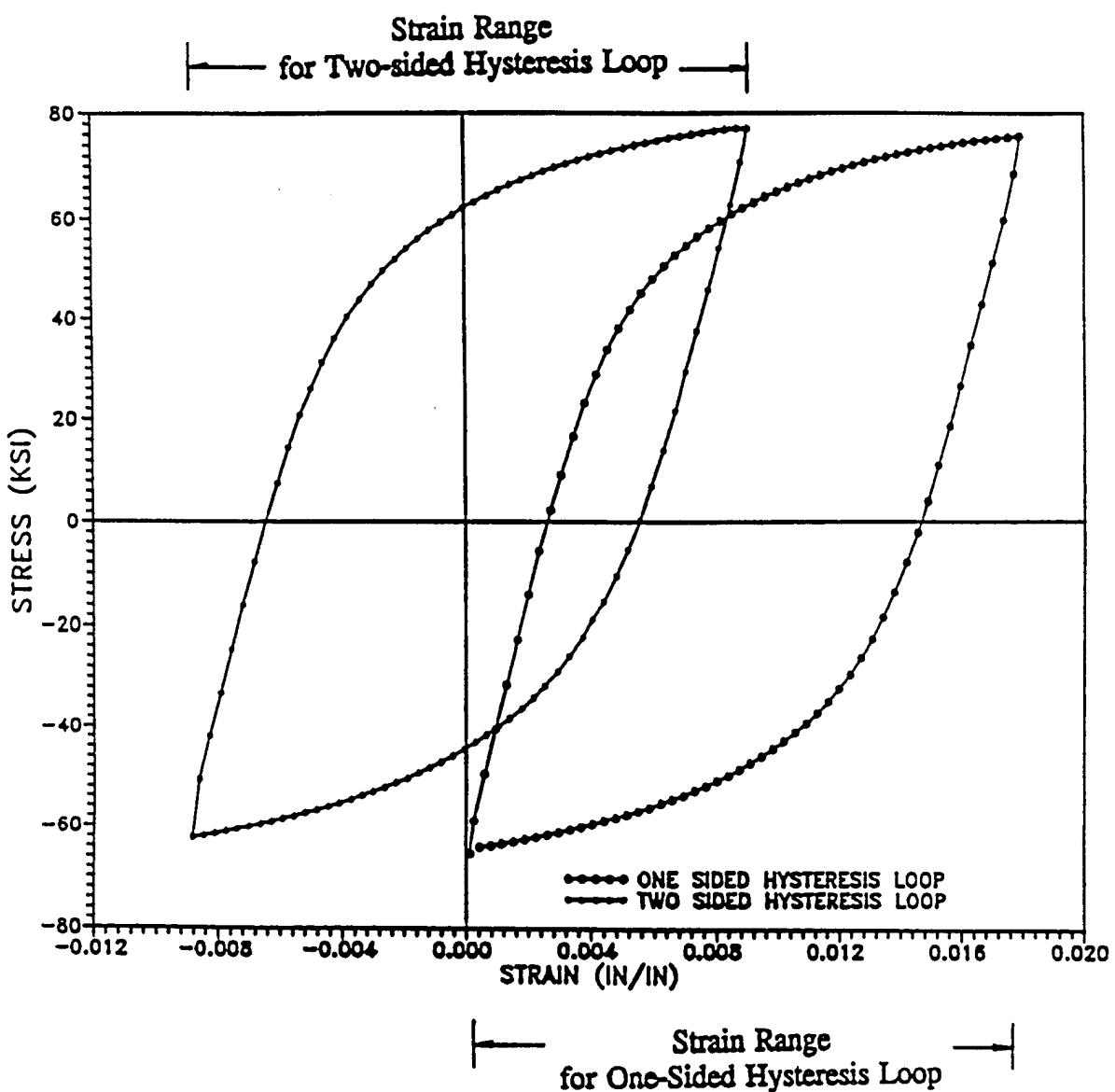
Figure 4.1. One-sided and Two-sided Hysteresis Loops
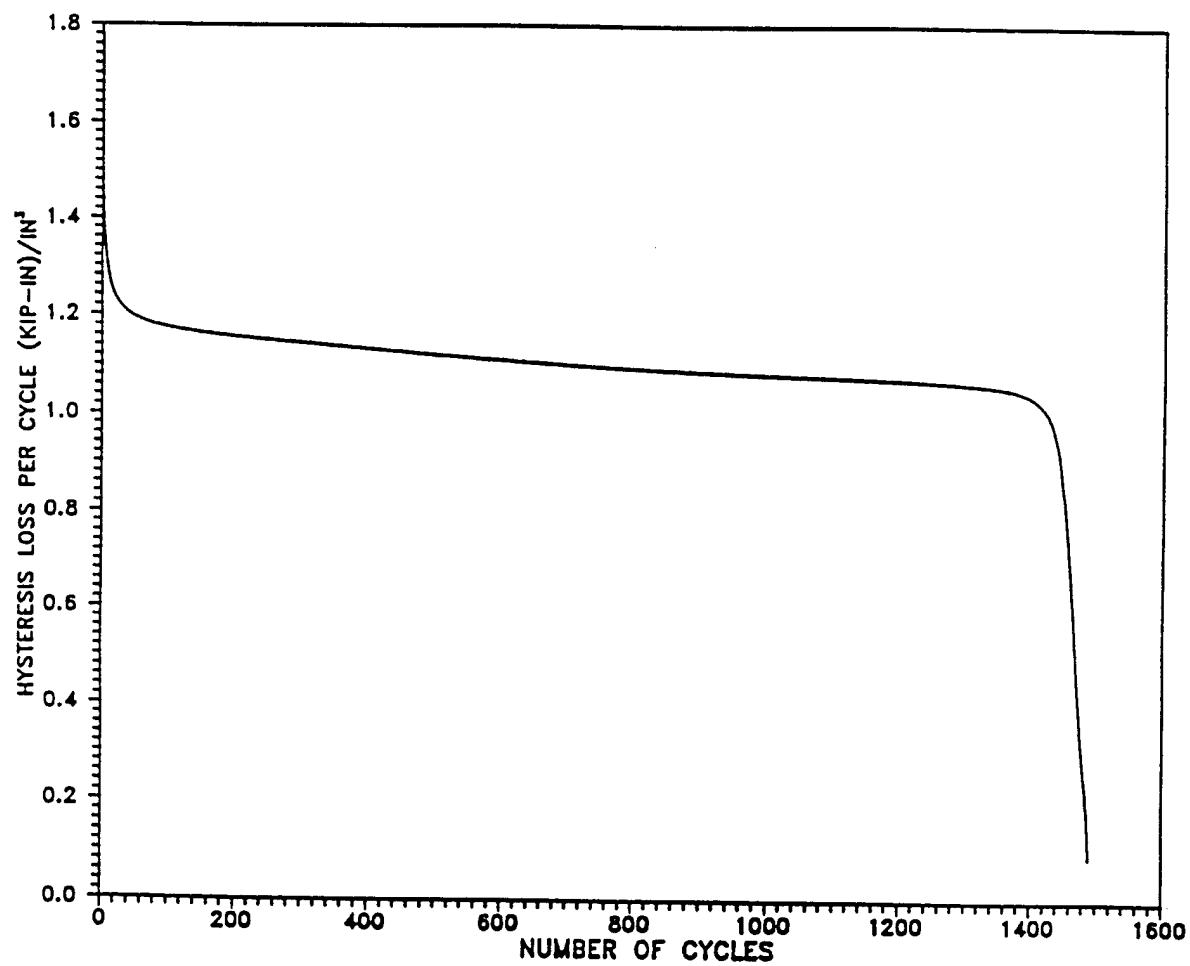
Figure 4.2. Hysteresis Loss per Cycle versus Number of Cycles
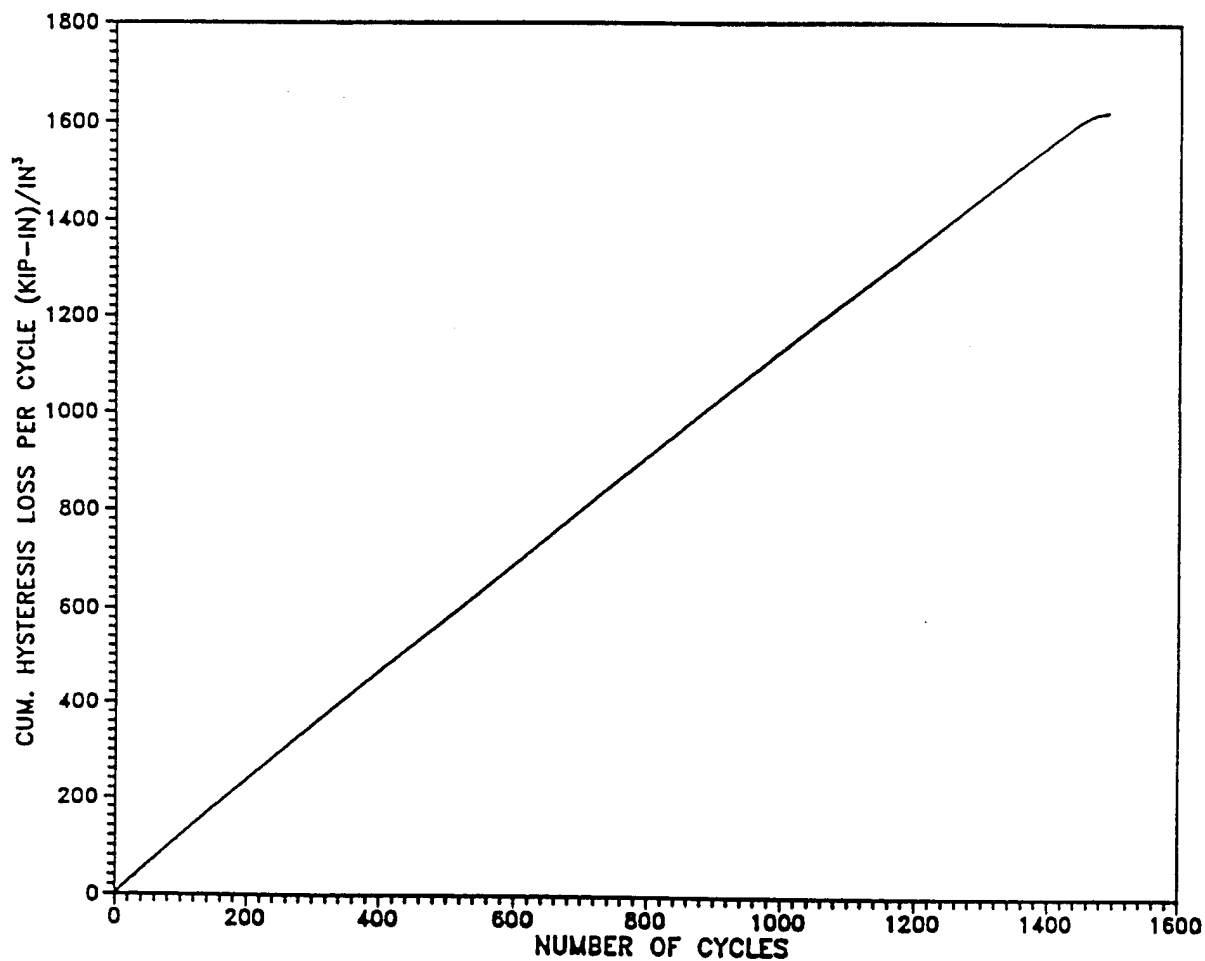
Figure 4.3. Cumulative Hysteresis Loss per Cycle versus Number of Cycles
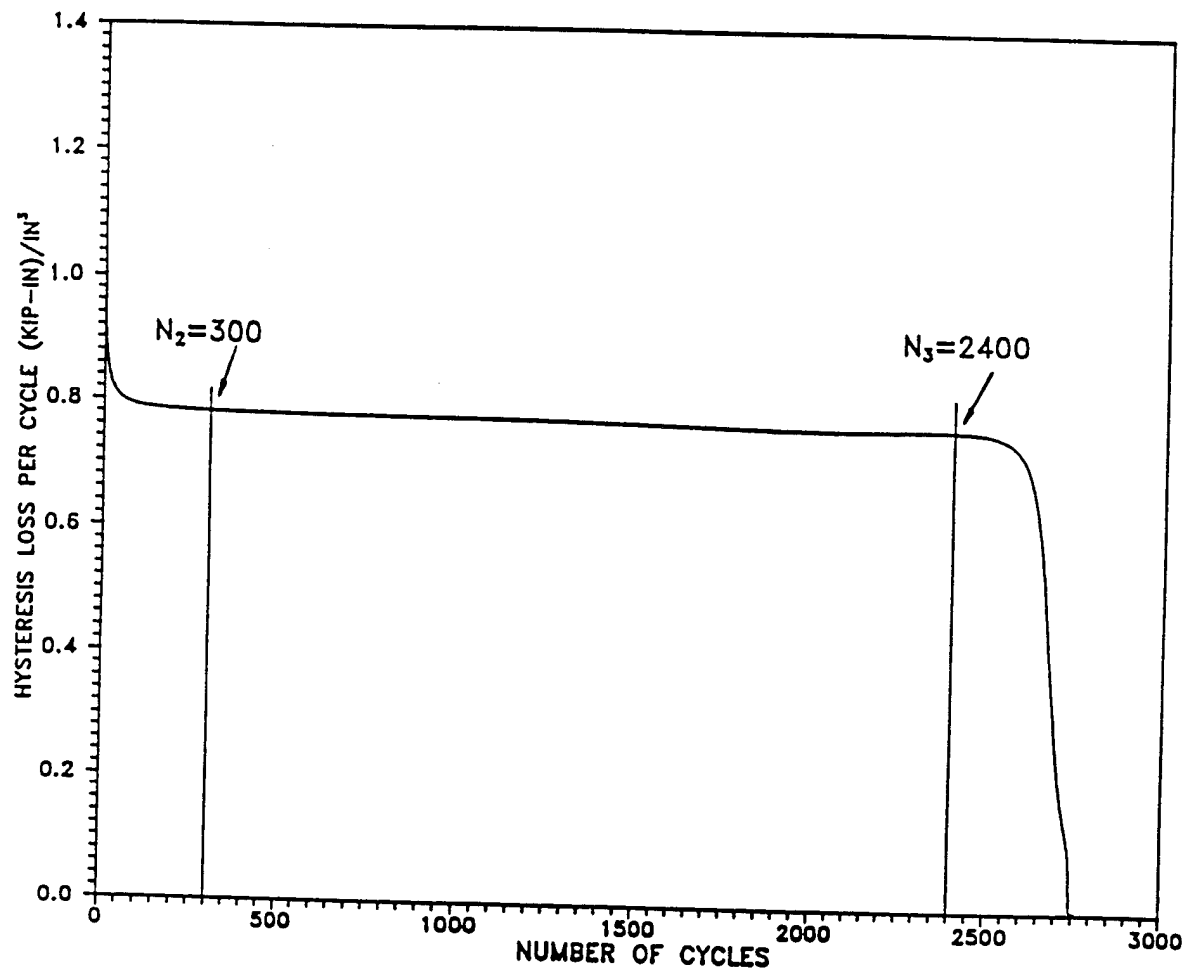
Figure 4.4. Definition of N_2 and N_3 Using Graph of Hysteresis Loss per Cycle

Figure 4.4 shows a typical graph of hysteresis loss per cycle versus number of cycles used to determine the two significant points: N_2 and N_3. N_2 is the point where the hysteresis loss per cycle becomes constant or nearly constant and N_3 is the point where the hysteresis loss per cycle starts to change rapidly.

One-sided Experiments (Non Alternating Cyclic Strain R=0)

In this set of experiments, specimens were cycled between 0 and ϵ_{max} to failure. In all, eighteen specimens were tested under this condition. The results are tabulated in Table A.1 of Appendix A.

Figure 4.5 and 4.6 show the graphs of the hysteresis loss per cycle versus number of cycles for strain ranges $\Delta\epsilon=0.014$ in/in and $\Delta\epsilon=0.008$ in/in, respectively. As may be observed from Figure 4.5, the hysteresis loss associated with individual loops began with a high value in the first cycle and then dropped to a nearly constant value after approximately $0.13N_f$ cycles had elapsed. Figure 4.6 on the other hand shows that the hysteresis loss began with a high value, just as in Figure 4.5, but then it dropped to a lower value than the constant value of the hysteresis loss and then increased to the constant value after approximately $0.13N_f$ cycles. The experiments conducted at a strain range $\Delta\epsilon \geq 0.014$ in/in invariably showed behavior similar to that shown in Figure 4.5. And, the experiments conducted at a strain range $\Delta\epsilon < 0.014$ in/in typically showed behavior similar to that shown in Figure 4.6. The number of cycles at which the hysteresis loss attained a constant value is hereinafter defined to be N_2.
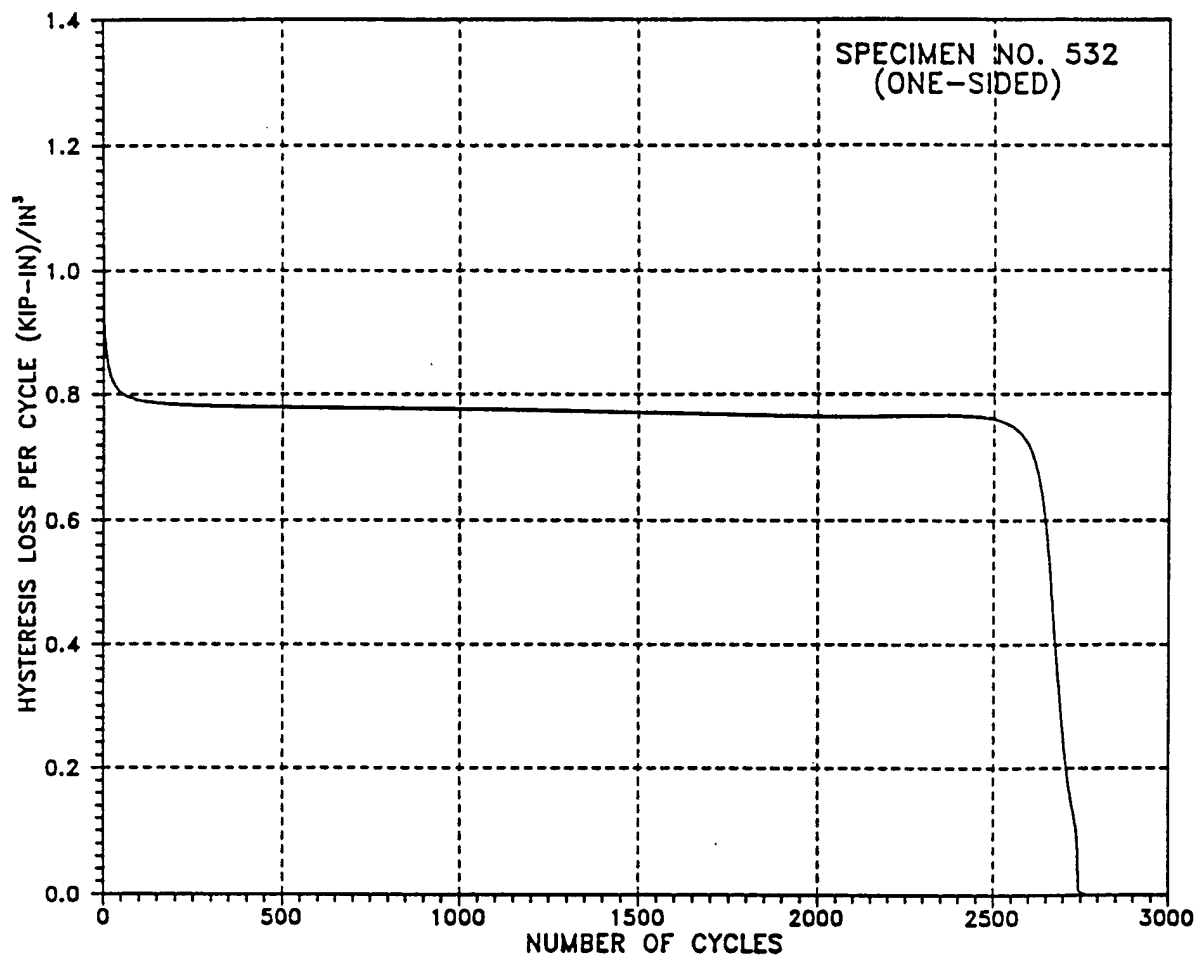
Figure 4.5. Hysteresis Loss per Cycle versus Number of Cycles, $\Delta\epsilon = 0.014$ in/in
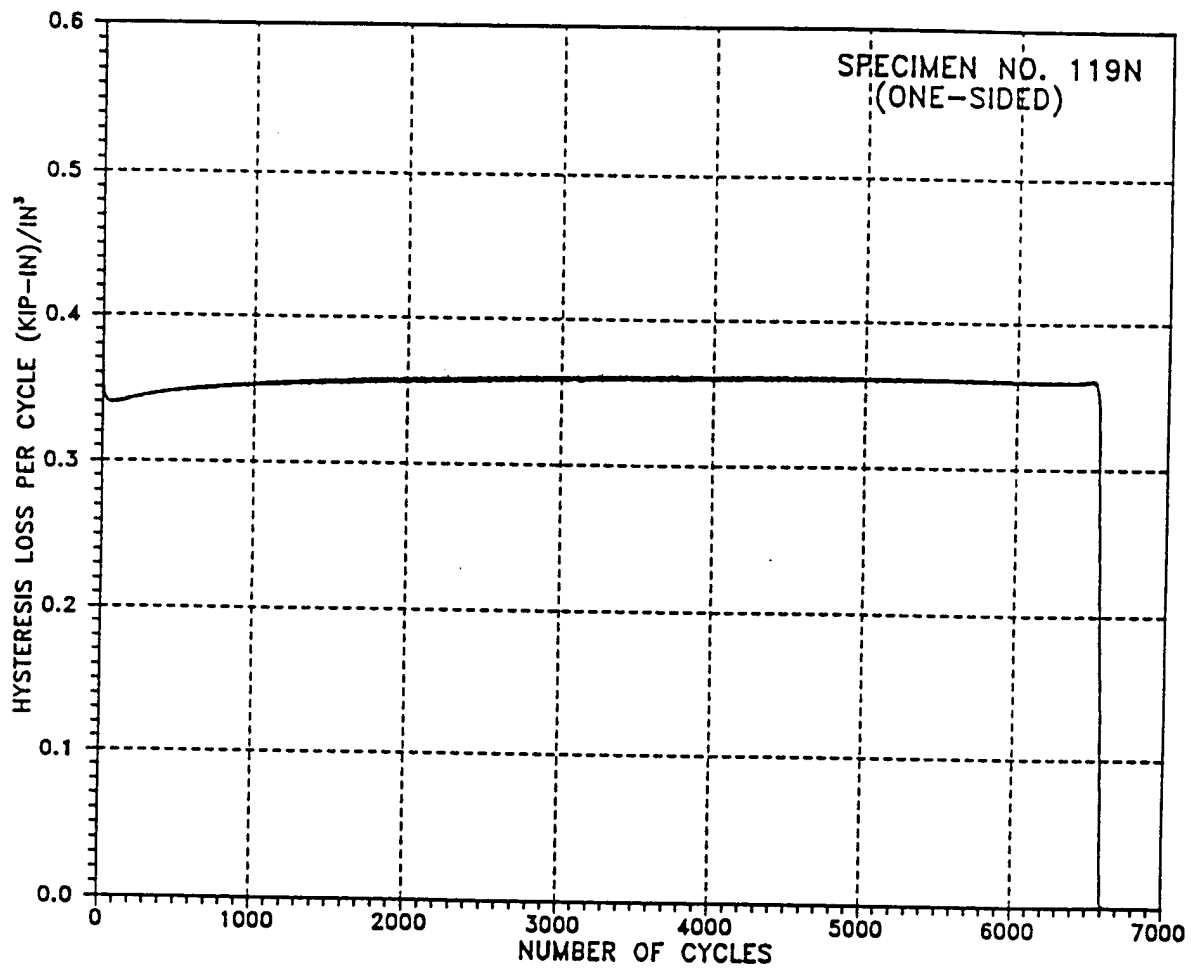
Figure 4.6. Hysteresis Loss per Cycle versus Number of Cycles, $\Delta\epsilon = 0.009$ in/in

After N_2 cycles of strain have been applied to the specimen, the hysteresis lossper cycle remained practically constant until N_3 cycles had elapsed. N_3 is hereinafter defined as the number of cycles at which the hysteresis loss began to deviate substantially from the constant value. Typically, this occurred when the number of cycles approached approximately $0.85N_f$. After this point, the hysteresis loss per cycle dropped significantly cycle after cycle until N_f, where the hysteresis loss per cycle approached zero.

Figures 4.7 and 4.8 show typical graphs of the cumulative hysteresis loss per cycle versus number of cycles for strain ranges $\Delta\epsilon = 0.014$ in/in and $\Delta\epsilon = 0.008$ in/in corresponding to Figures 4.5 and 4.6. As may be observed from these two figures, the graphs of the cumulative hysteresis loss per cycle versus number of cycles were essentially straight lines, which, of course, confirms the observation that the hysteresis loss per cycle has nearly a constant value with the exception of the initial and the final span of cycles which do not exceed 15% of N_f. The slopes of these lines yield the average hysteresis losses per cycle for the particular specimen. An important observation, that the total hysteresis loss can not be equated to the cumulative damage sustained by the material, can be made from a comparison of Figure 4.7 with Figure 4.8. As these graphs show, the specimen cycled at the higher strain range had a somewhat smaller total hysteresis energy dissipation than the specimen cycled at the lower strain range. Hence, if total hysteresis loss can be equated to damage, then the specimen cycled at the higher strain range should apparently live longer than the one cycled at the lower strain range. This is simply not true.

Another important observation can be inferred from Figure 4.9. This figure shows the graph of the hysteresis loss per cycle versus number of cycles for three specimens

subjected to a strain range of $\Delta\epsilon = 0.007$ in/in. The number of cycles to failure, N_f, for these specimens were 7739, 9812 and 12112 cycles, respectively. The corresponding average hysteresis loss per cycle values were: 0.190, 0.207 and 0.197 (kip-in)/(in^3) per cycle, respectively. These results showed that the average hysteresis loss per cycle is not dependent on the number of cycles to failure, N_f, for a set of experiments conducted at a particular strain range. However, the average hysteresis loss per cycle does depend on the strain range. This observation is treated in more detail later in this chapter.

Figure 4.10 shows a conventional Strain Range versus Life (S-N) diagram obtained from the data reported in Table A.1 of Appendix A. The development of a 'knee' in the S-N diagram may be observed in Figure 4.10. This 'knee' has also been observed by many other researchers. The data shown in this figure may be fitted by the equation:

$$\Delta\epsilon = 0.119 \ N_f^{-0.295} \tag{4.1}$$

One of the important results obtained in this investigation is the discovery of a relatively simple relationship between the average hysteresis loss per cycle, $<\Delta U_i(\epsilon)>$ and the number of cycles to failure, N_f. This is shown in the Figure 4.11. The data shown in this figure may be fitted by the equation:

$$<\Delta U_i> = 43.095 \ N_f^{-0.559} \tag{4.2}$$
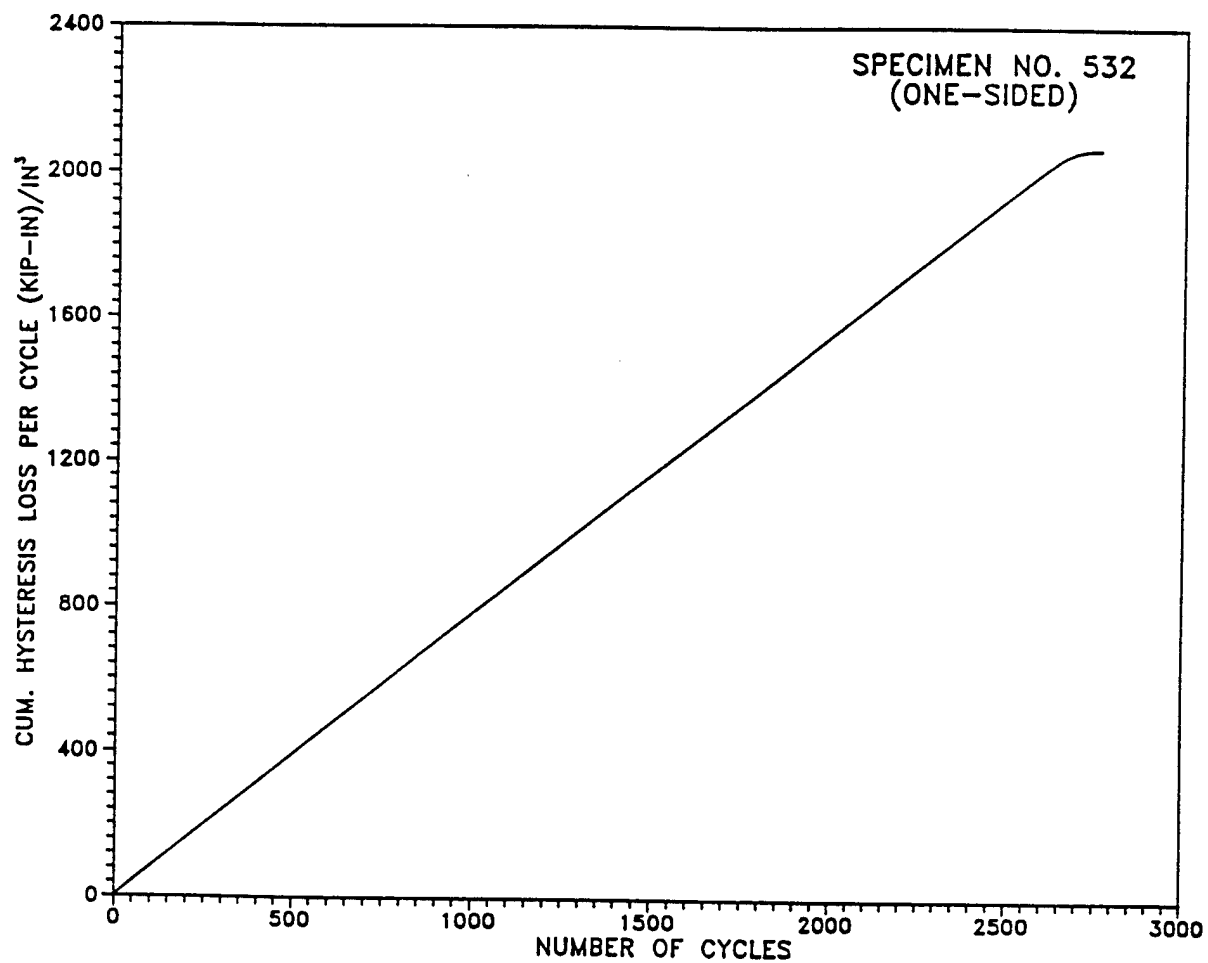
Figure 4.7. Cumulative Hysteresis Loss per Cycle

versus Number of Cycles, $\Delta\epsilon=0.014$ in/in
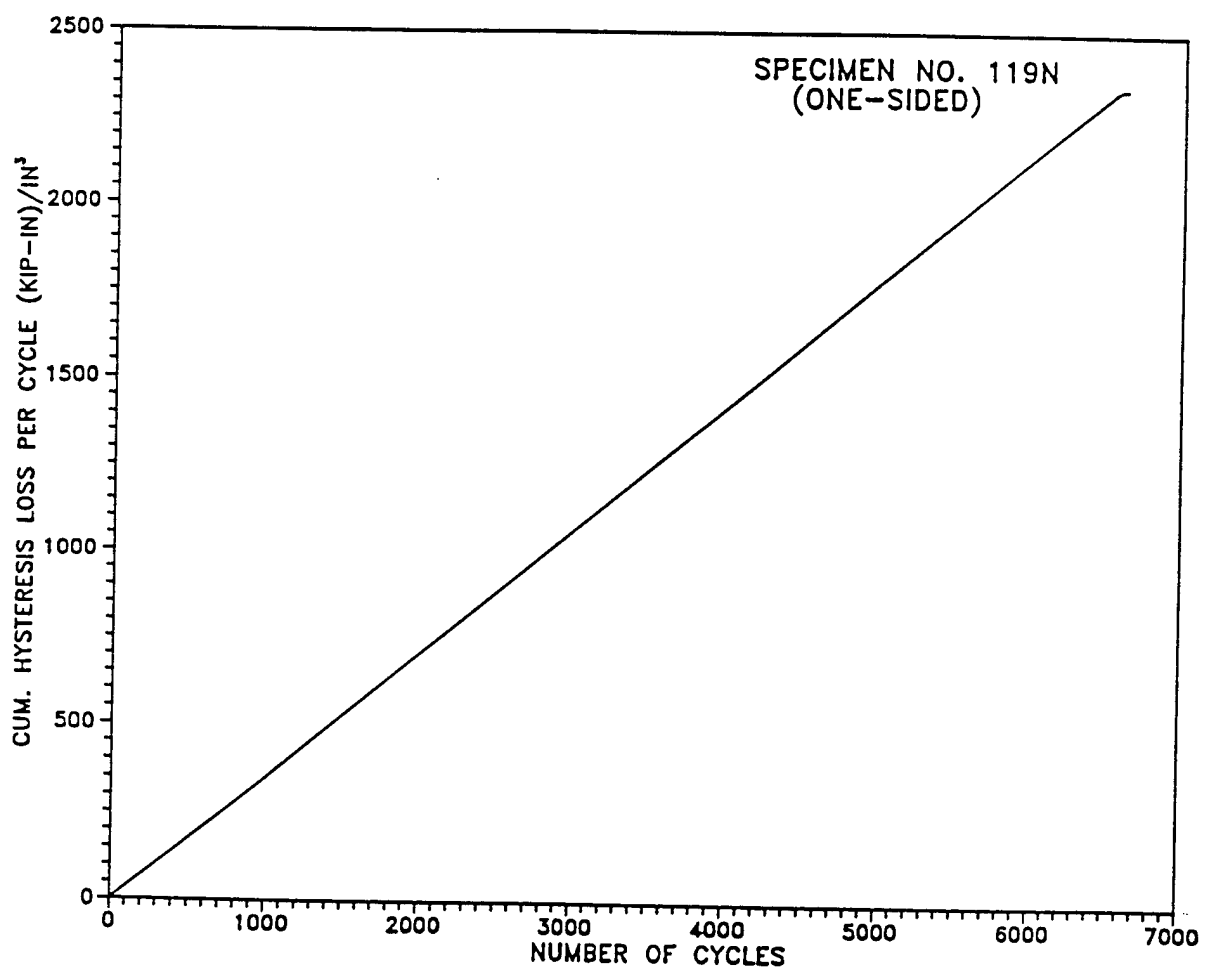
Figure 4.8. Cumulative Hysteresis Loss per Cycle

versus Number of Cycles, $\Delta\epsilon = 0.009$ in/in
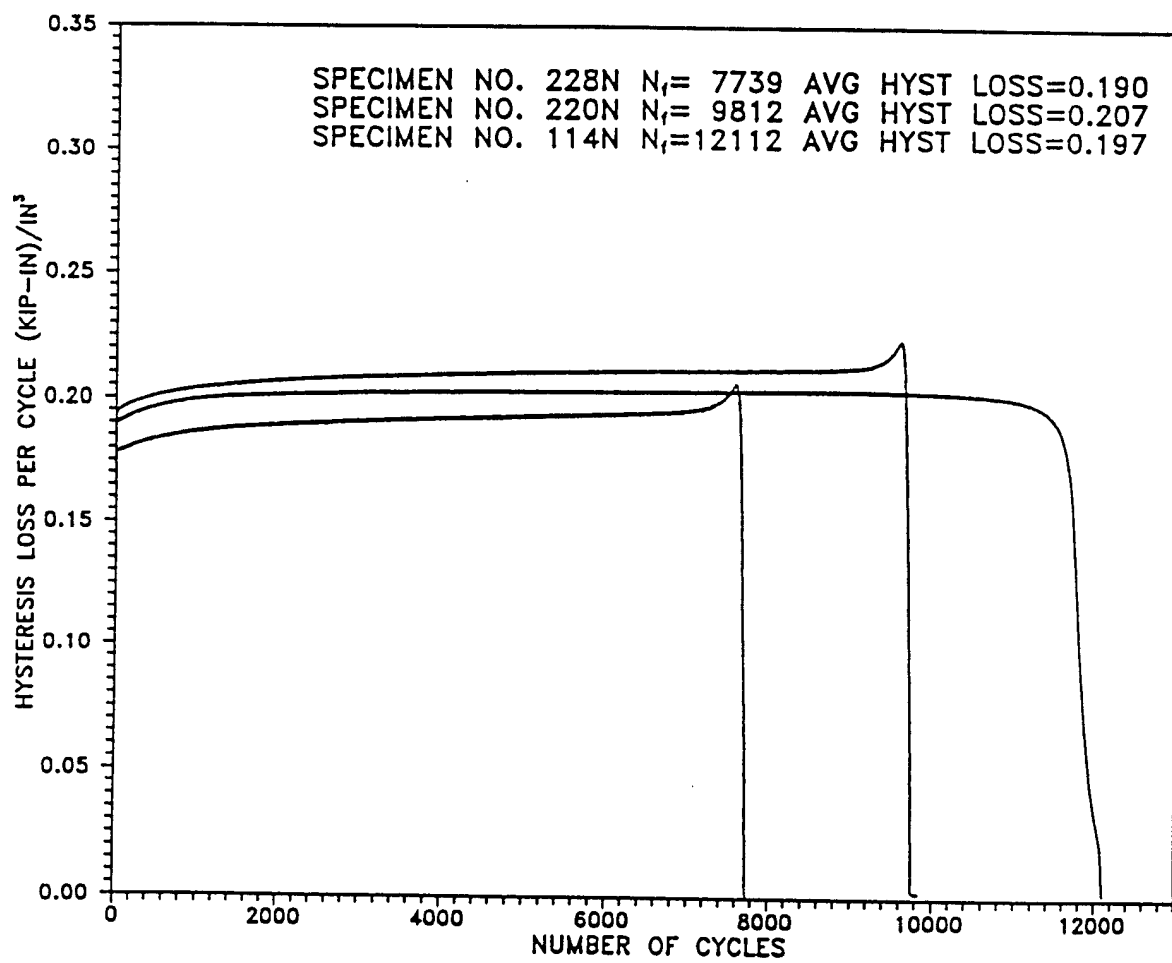
Figure 4.9. Hysteresis Loss per Cycle versus Number of Cycles, $\Delta\epsilon=0.007$ in/in

This equation clearly shows that as the number of cycles to failure, N_f, approaches infinity, the average hysteresis loss per cycle, $<\Delta U_i>$, approaches zero. Therefore, it may be concluded that $<\Delta U_i>$ can be used to identify an endurance limit for this material.

The graph of data from Table A.1 of Appendix A connecting cumulative hysteresis energy loss at failure, or the total hysteresis energy loss, $\sum \Delta U_i$, to the number of cycles to failure, N_f, is shown the Figure 4.12. As may be observed from this graph, the function which is used to fit the data is monotonically increasing. This means that as N_f approaches infinity, the total energy dissipated must also approach infinity. As mentioned earlier, this can not be true. Hence, the assertion that total hysteresis energy can not in and of itself be equated to cumulative damage is confirmed. The relation between $\sum \Delta U_i$ and N_f may be represented by the equation:

$$\sum \Delta U_i = 46.875 \ N_f^{0.431} \qquad (4.3)$$

Two-sided Experiments (Completely Alternating Cyclic Strain R=-1)

In this set of experiments, specimens were cycled between the strain limits ϵ_{min} and ϵ_{max} at zero mean strain to failure. In all, eighteen specimens were tested under this set of conditions. The results are tabulated in Table A.2 of Appendix A.

The graphs of the hysteresis loss per cycle versus number of cycles for the two-sided experiments shown in Figures 4.13 and 4.14 displayed behavior similar to that shown in Figures 4.5 and 4.6 for the one-sided experiments. As may be observed from Figure 4.13, the hysteresis loss associated with individual loops began with a high value in the first cycle

$$\Delta \epsilon = 0.119 \; N_f^{-0.295} \qquad\qquad r^2 = 0.74 \qquad\qquad (4.1)$$
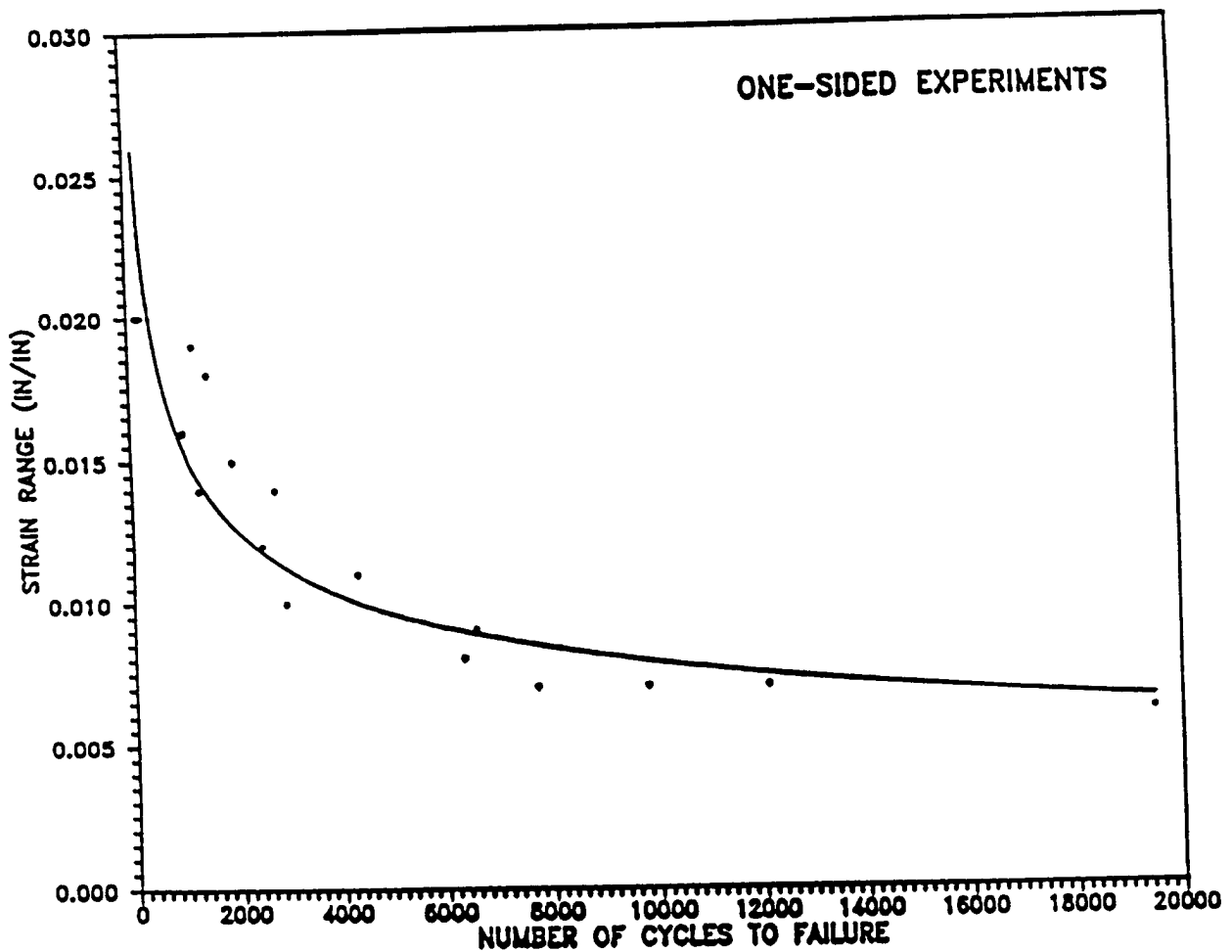
Figure 4.10. Strain Range, $\Delta \epsilon$, versus Number of Cycles to Failure, N_f

$$<\Delta U_i> = 43.095 \, N_f^{-0.559} \qquad\qquad r^2=0.73 \qquad\qquad (4.2)$$
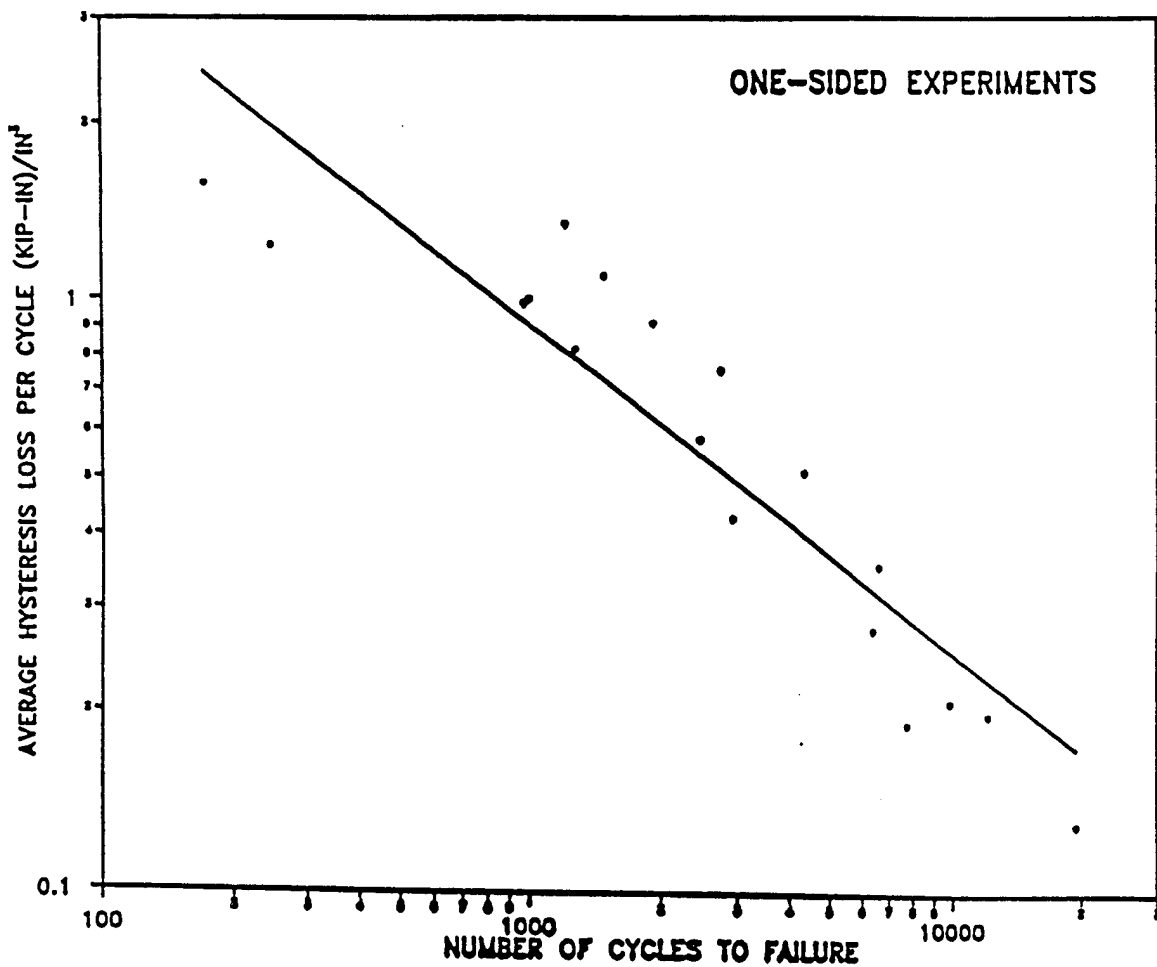
Figure 4.11. Average Hysteresis Loss per Cycle, $<\Delta U_i>$,

versus Number of Cycles to Failure, N_f

$$\sum \Delta U_i = 46.875 \, N_f^{0.431} \qquad\qquad r^2 = 0.55 \qquad\qquad (4.3)$$
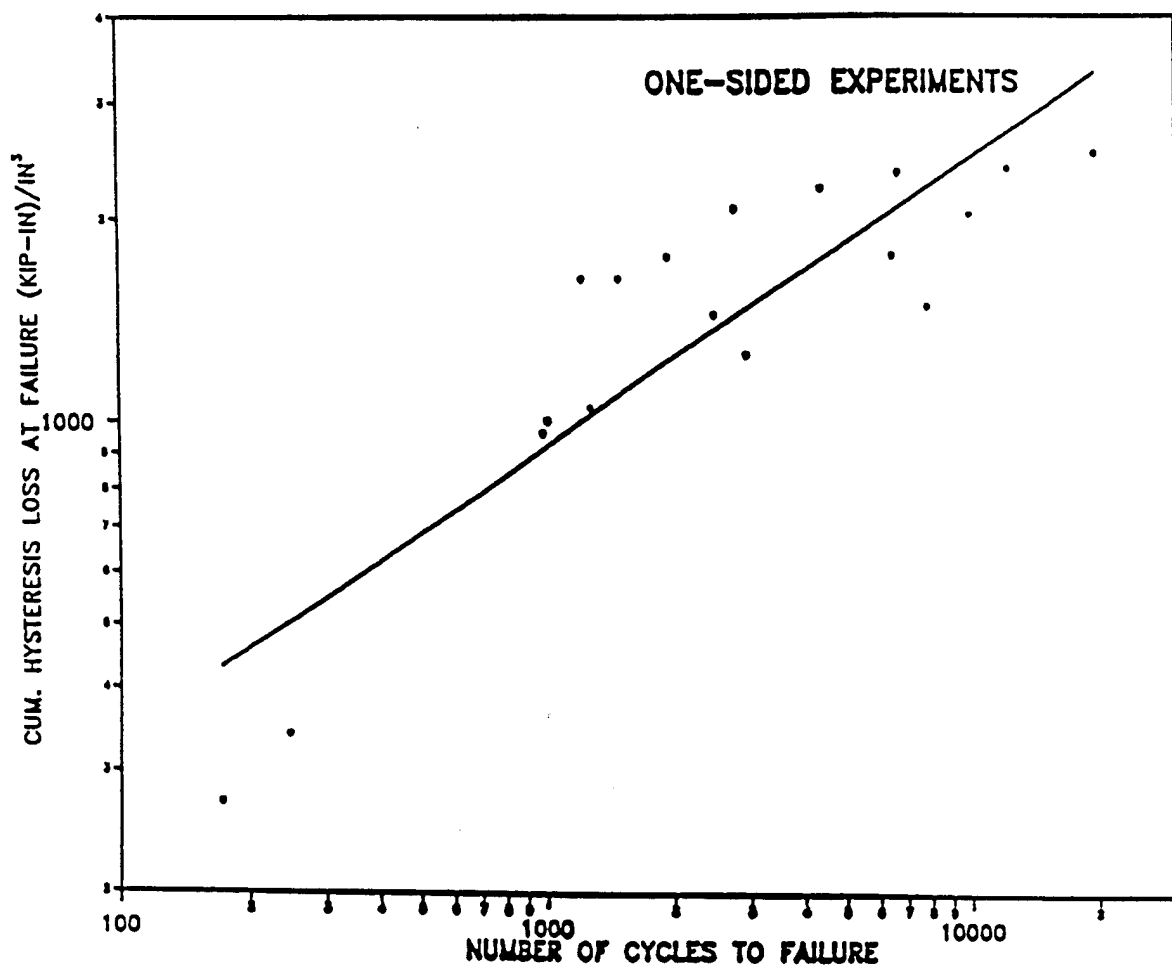
Figure 4.12. Cumulative Hysteresis Loss at Failure, $\sum \Delta U_i$,

versus Number of Cycles to Failure, N_f

and then dropped to a nearly constant value after approximately $0.13N_f$ cycles had occurred. In contrast, Figure 4.14 shows that the hysteresis loss began with a high value, just as in Figure 4.5, but then it dropped to a lower value than the constant value of the hysteresis loss and then increased to the constant value after approximately $0.13N_f$ cycles had elapsed. The experiments conducted at strain ranges $\Delta\epsilon > 0.011$ in/in invariably showed behavior similar to that shown in Figure 4.13. And, the experiments conducted at strain ranges $\Delta\epsilon \leq 0.011$ in/in showed behavior similar to that shown in Figure 4.14. Again, just as in the one-sided tests, the number of cycles at which the hysteresis loss attained a constant value is defined as N_2.

After N_2 cycles had elapsed, the hysteresis loss per cycle remained practically constant until N_3 cycles had elapsed. Just as in the one-sided experiments, N_3 is defined as the number of cycles where the hysteresis loss began to deviate substantially from the constant value. Typically, this point was observed to occur at approximately $0.85N_f$ cycles. After this point, the hysteresis loss per cycle decreased significantly for each cycle until N_f was reached, where the hysteresis loss per cycle decreased to nearly zero.

The graphs of the cumulative hysteresis loss per cycle versus number of cycles for the two-sided experiments shown in Figures 4.15 and 4.16 displayed behavior similar to that shown in Figures 4.7 and 4.8 for the one-sided experiments which were essentially straight lines. Again, the observation was confirmed that the hysteresis loss per cycle is nearly a constant value with the exception of the group of initial and final cycles which did not span more than $15\%N_f$. Again, it is clear that the total hysteresis energy dissipation can not be equated to cumulative fatigue damage.
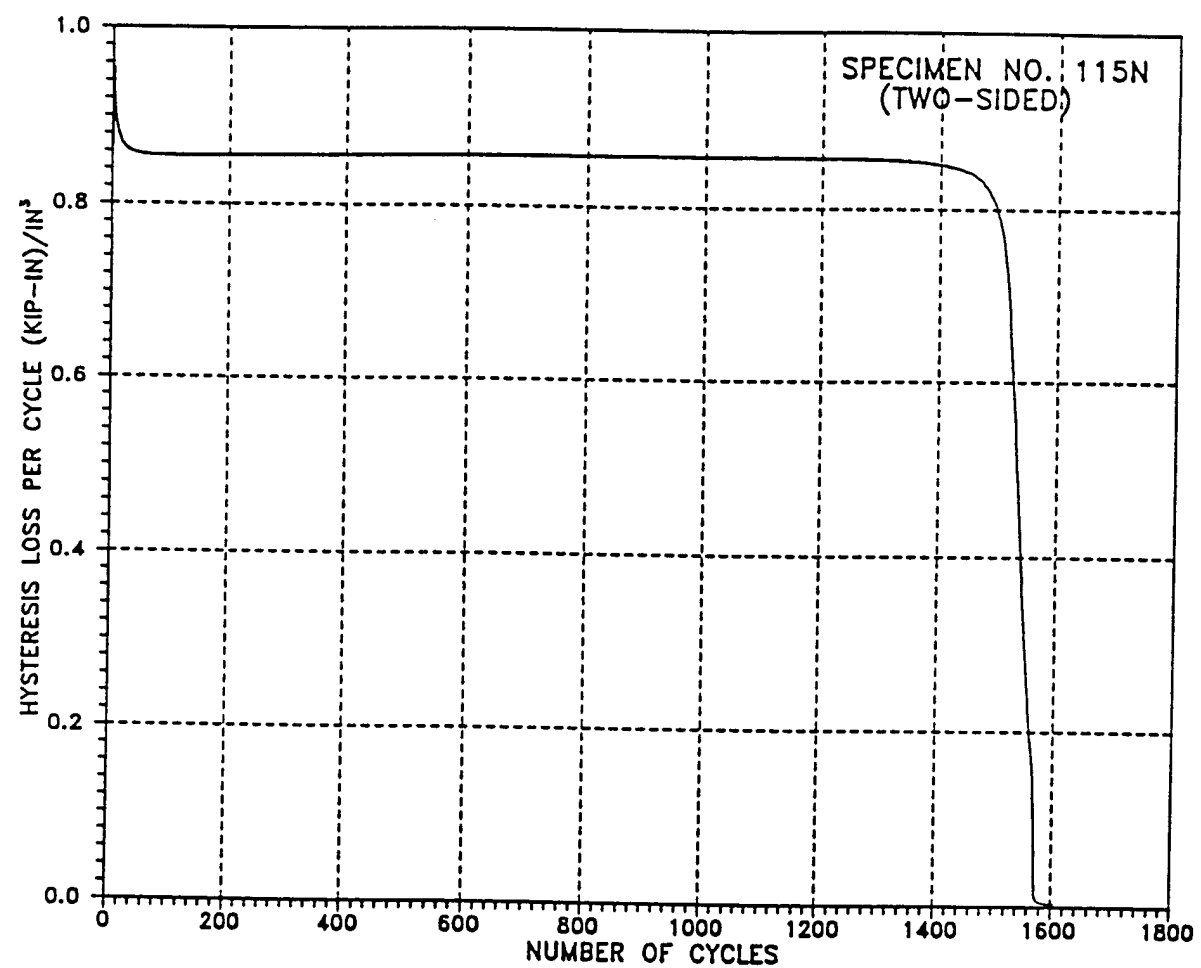
Figure 4.13. Hysteresis Loss per Cycle versus Number of Cycles, $\Delta\epsilon=0.014$ in/in
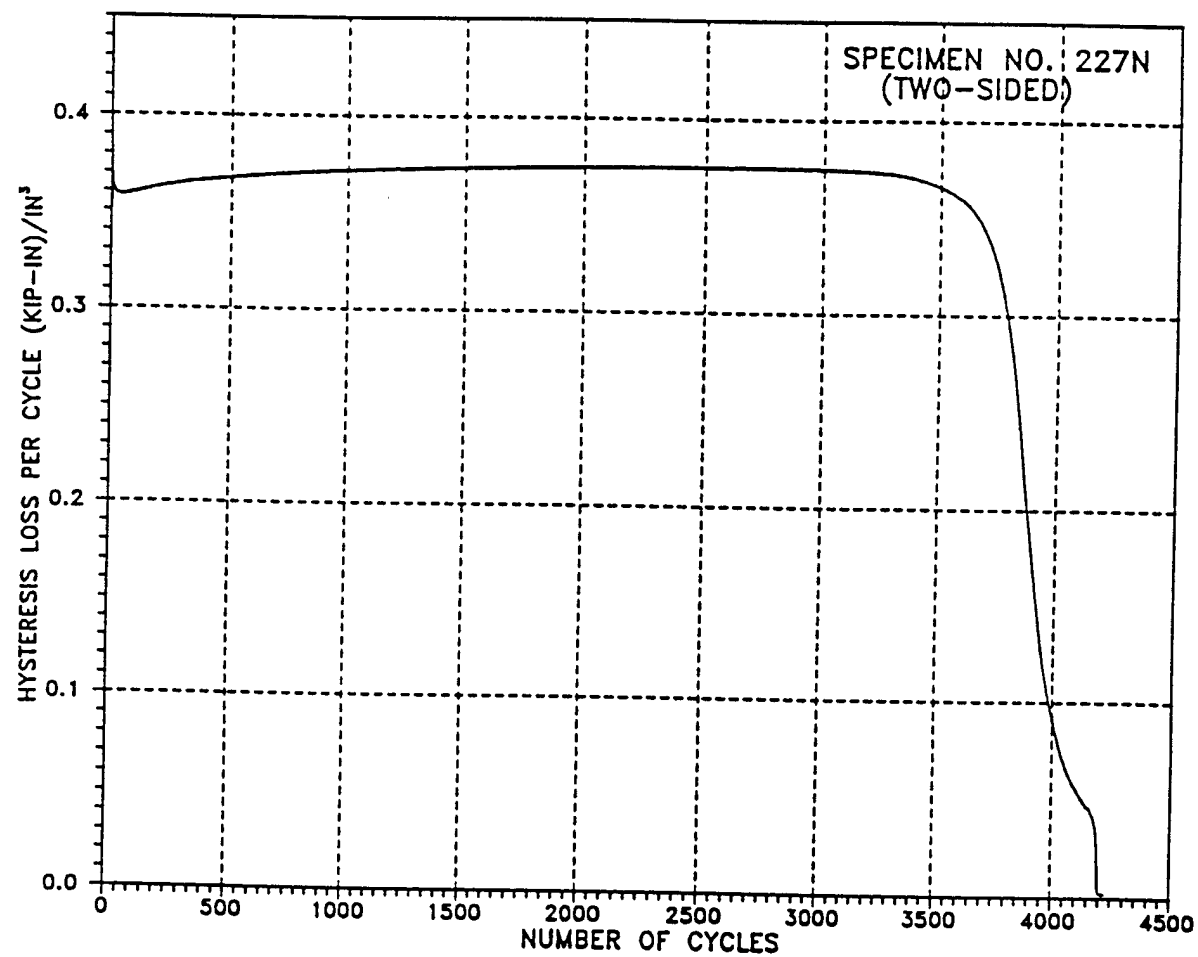
Figure 4.14. Hysteresis Loss per Cycle versus Number of Cycles, $\Delta\epsilon = 0.009$ in/in

Figure 4.17 presents a conventional Strain-Life diagram obtained for the two-sided experimental data given in Table A.2 of Appendix A. The data can be represented by the equation:

$$\Delta\epsilon = 0.303 \ N_f^{-0.410} \qquad (4.4)$$

The relationship between the average hysteresis loss per cycle, $<\Delta U_i(\epsilon)>$ and the number of cycles to failure, N_f is given in Figure 4.18. This data may be represented by the equation:

$$<\Delta U_i> = 336.329 \ N_f^{-0.808} \qquad (4.5)$$

As in the case of the one-sided experiments, as the number of cycles to failure, N_f, approaches infinity, the average hysteresis loss per cycle, $<\Delta U_i>$, approaches zero. Therefore, it may be concluded that $<\Delta U_i>$ can be used to identify the endurance limit for this material. This is explained in detail later with the combined results.

A graph of cumulative hysteresis loss at failure, or the total hysteresis loss, $\sum \Delta U_i$, versus number of cycles to failure, N_f, is shown in Figure 4.19. As may be observed from this figure, the function used to fit the data is a monotonically increasing one which means that as N_f approaches infinity, the total energy dissipated also approaches infinity. As mentioned earlier, this can not be true. Hence, the assertion that total hysteresis energy can not be equated to the cumulated total damage is confirmed. The relationship between $\sum \Delta U_i$ and N_f may be represented by the equation:
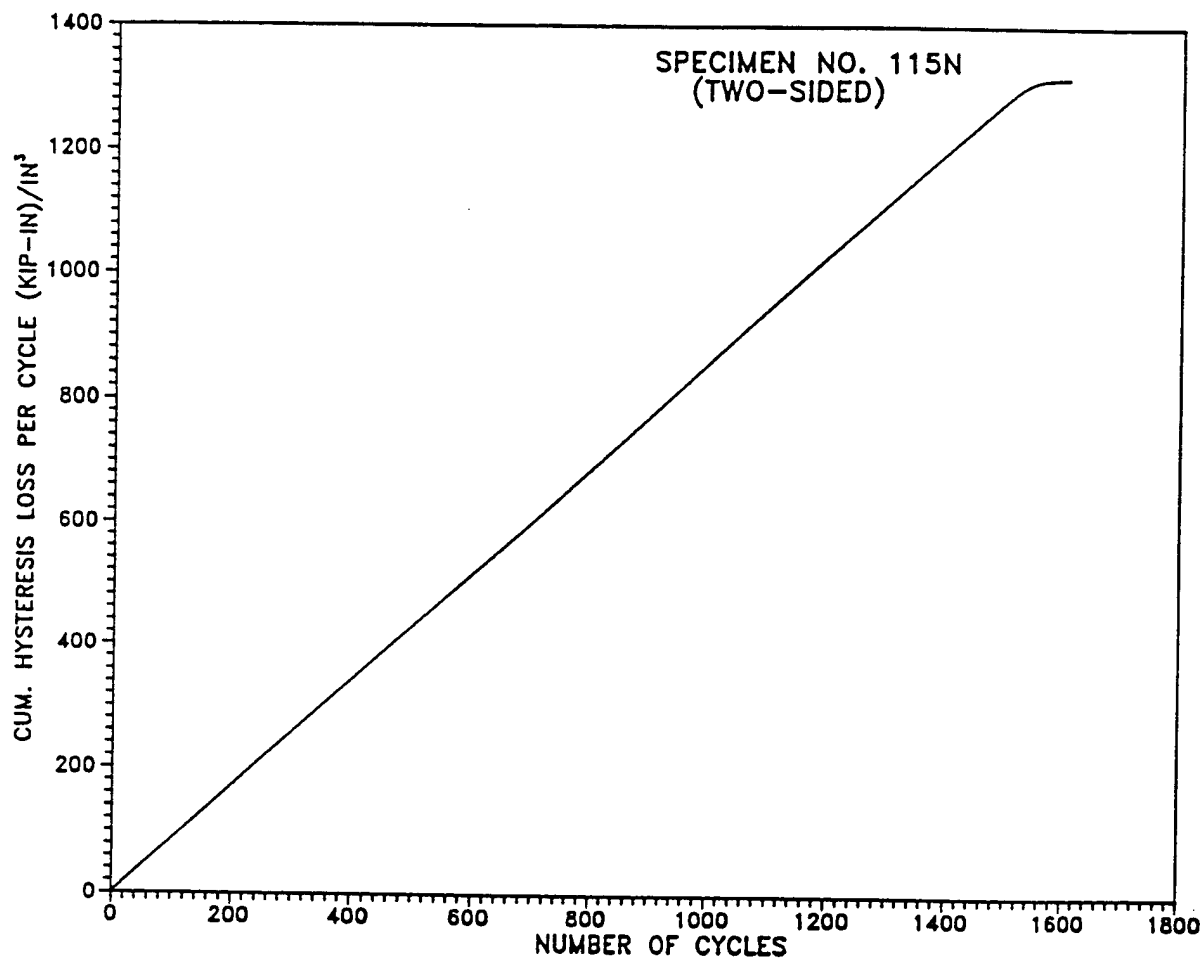
Figure 4.15 Cumulative Hysteresis Loss per Cycle versus Number of Cycles,

$\Delta\epsilon = 0.014$ in/in
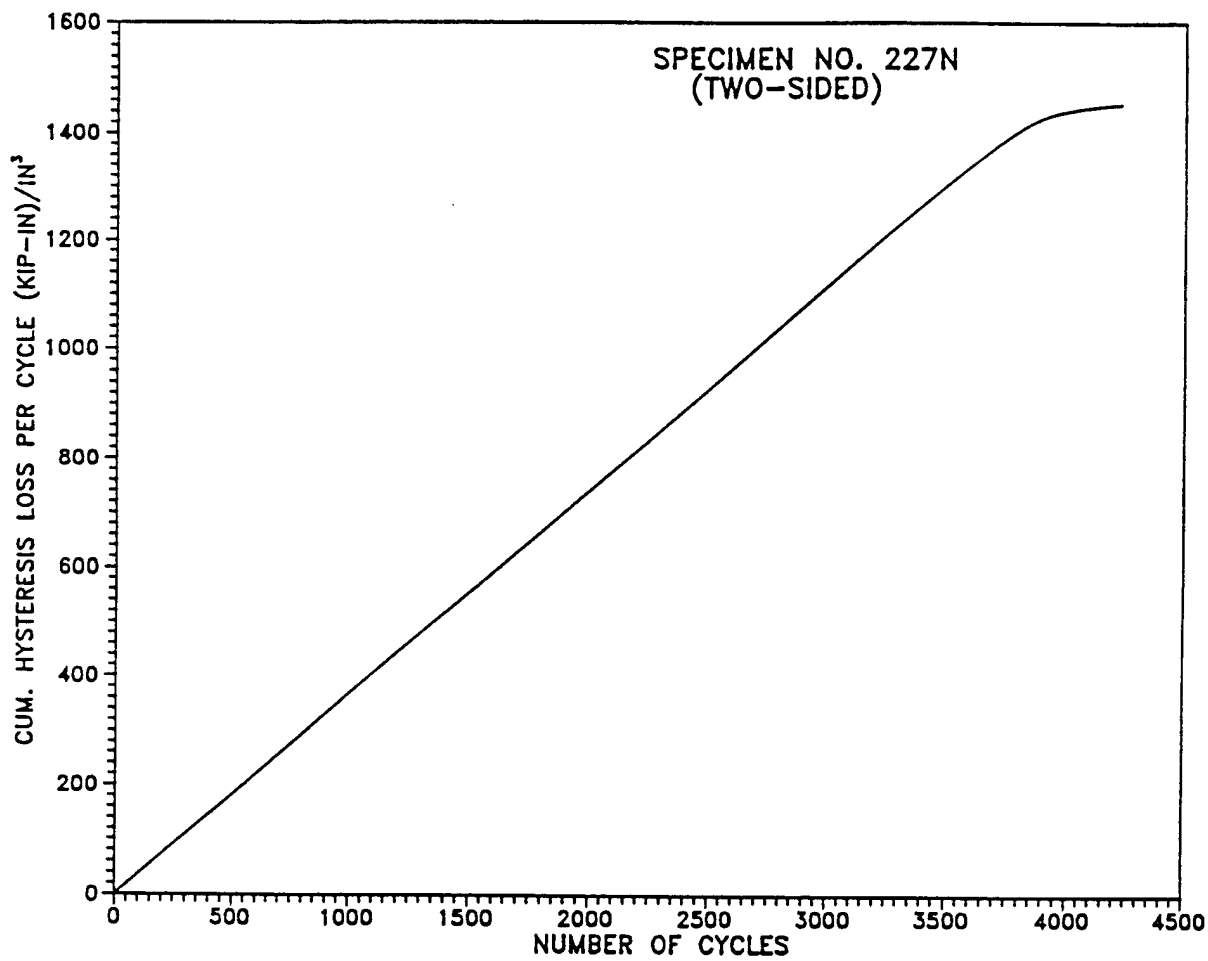
Figure 4.16 Cumulative Hysteresis Loss per Cycle versus Number of Cycles,

$\Delta\epsilon = 0.009$ in/in

$$\sum_i \Delta U_i = 336.172 \ N_f^{0.192} \qquad (4.6)$$

Combined Results (One-Sided and Two-sided Experiments)

A comparison of the results from the one-sided experiments and the corresponding results from the two-sided experiments reveals that these two entirely different sets of data display several kinds of identical behavior. This fact indicates that it may be possible to combine these two sets of data in certain ways. The following figures show a combination of the results from the one-sided and the two-sided experiments.

Figure 4.20 shows the graph of strain range, $\Delta\epsilon$, versus number of cycles to failure, N_f for the combined data. The data shown in this figure may be represented by the equation:

$$\Delta\epsilon = 0.166 \ N_f^{-0.336} \qquad (4.7)$$

The following equation has been fitted to the combined one-sided and two-sided data of average hysteresis loss per cycle, $<\Delta U_i>$ versus number of cycles to failure, N_f.

$$<\Delta U_i> = 90.409 \ N_f^{-0.648} \qquad (4.8)$$

The data together with a graph of equation 4.8 is shown in Figure 4.21. Here, again, it may be seen that as N_f approaches infinity, $<\Delta U_i>$ approaches zero. Hence, the assertion that $<\Delta U_i>$ can be used as an index of the endurance limit is once again confirmed.

An interesting relationship between the average hysteresis loss per cycle, $<\Delta U_i>$, and the strain range, $\Delta\epsilon$, for the combined data is given in Figure 4.22. This relationship may be represented by the equation:

$$<\Delta U_i> = 92.555\ \Delta\epsilon - 0.468 \tag{4.9}$$

Equation 4.2 indicates that $<\Delta U_i>$ approaches zero as N_f approaches infinity. If this assertion is used in Equation 4.9, it is possible to estimate the endurance limit for this material. Substituting $<\Delta U_i> = 0$ in Equation 4.9 gives $\Delta\epsilon_{el} \cong 0.005 \pm 0.0008$ in/in. Compared to previous experiments, this value of the endurance limit appears to overestimate the actual value. It is most likely that this overestimation results from the strain range selected for this particular set of experiments. All of the experiments of this investigation were conducted at strain ranges which varied between 0.006 in/in and 0.020 in/in. With a set of experiments distributed over a wider group of strain ranges, this overestimate may disappear. As shown earlier, the hysteresis loss, ΔU_i, becomes approximately constant or stable after $N_2 = 0.13 N_f$ cycles have occurred. Hence, it may not be necessary to conduct fatigue experiments until failure occurs. The values of the hysteresis loss per cycle, ΔU_i, observed just after N_2 cycles have elapsed can very well be used as an approximation to the average hysteresis loss per cycle, $<\Delta U_i>$, to construct graphs similar to the average hysteresis loss per cycle, $<\Delta U_i>$, versus the strain range, $\Delta\epsilon$, graph given in Figure 4.22. If this is done, then a tremendous amount of experimental work is avoided.

$$<\Delta U_i> = 336.329 \ N_f^{-0.808} \qquad\qquad r^2 = 0.94 \qquad\qquad (4.5)$$
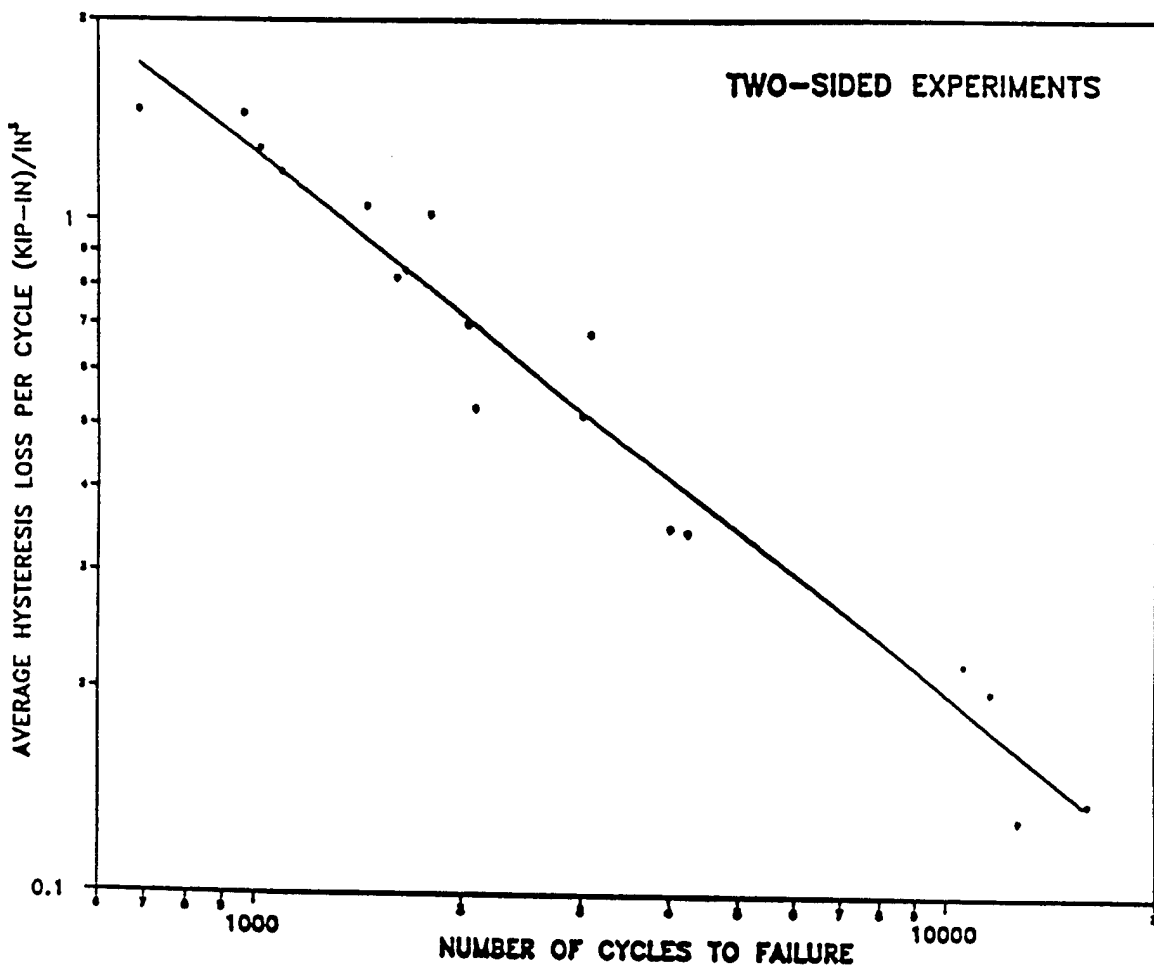
Figure 4.18. Average Hysteresis Loss per Cycle, $<\Delta U_i>$,

versus Number of Cycles to Failure, N_f

$$\sum \Delta U_i = 336.172 \, N_f^{0.192} \qquad\qquad r^2 = 0.59 \qquad\qquad (4.6)$$
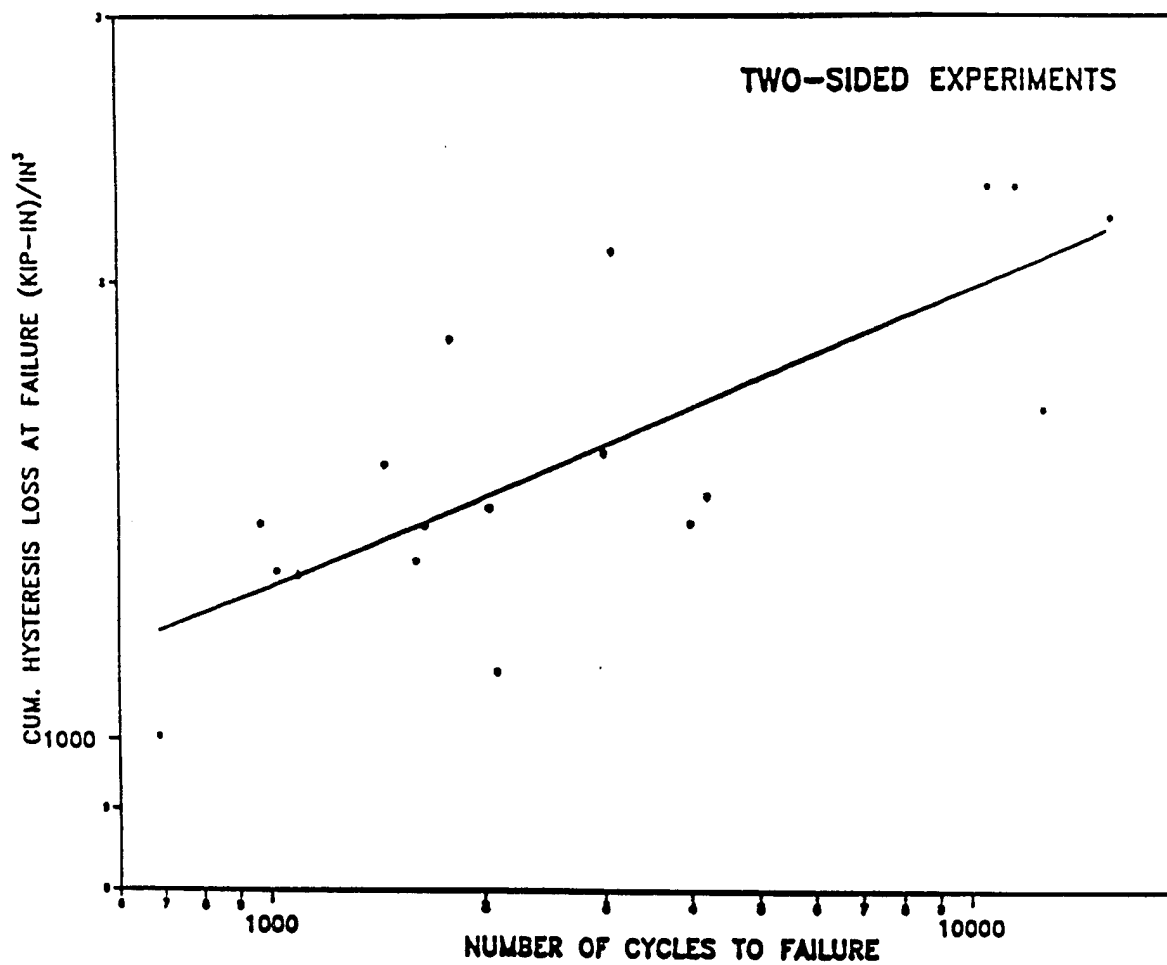
Figure 4.19. Cumulative Hysteresis Loss at Failure, $\sum \Delta U_i$,

versus Number of Cycles to Failure, N_f

Figure 4.23 gives a graph of cumulative hysteresis loss at failure, $\sum \Delta U_i$, versus the number of cycles to failure, N_f, for the combined data. The following equation may be used to fit the data:

$$\sum \Delta U_i = 95.396 \ N_f^{0.346} \tag{4.10}$$

A comparison of N_2 and N_3 with respect to N_f has led to two very important observations. Figure 4.24 shows a graph of N_2 versus N_3. The following equation represents the data shown in this figure:

$$N_2 = 0.129 \, N_f \tag{4.11}$$

This simple empirical equation, when transformed in the following form, can be used to predict fatigue failure from experiments designed to measure hysteresis loss per cycle versus number of cycles to failure.

$$N_f = 7.752 \, N_2 \tag{4.12}$$

Equation 4.12 was found to yield conservative estimates for 76% of the data acquired in this investigation. Some 66% of the data were found to lie within a band whose width is $\pm 10\%$ of the N_f value predicted by means of Equation 4.12.

$$\Delta\epsilon = 0.166 \ N_f^{-0.336} \qquad\qquad r^2 = 0.72 \qquad\qquad (4.7)$$
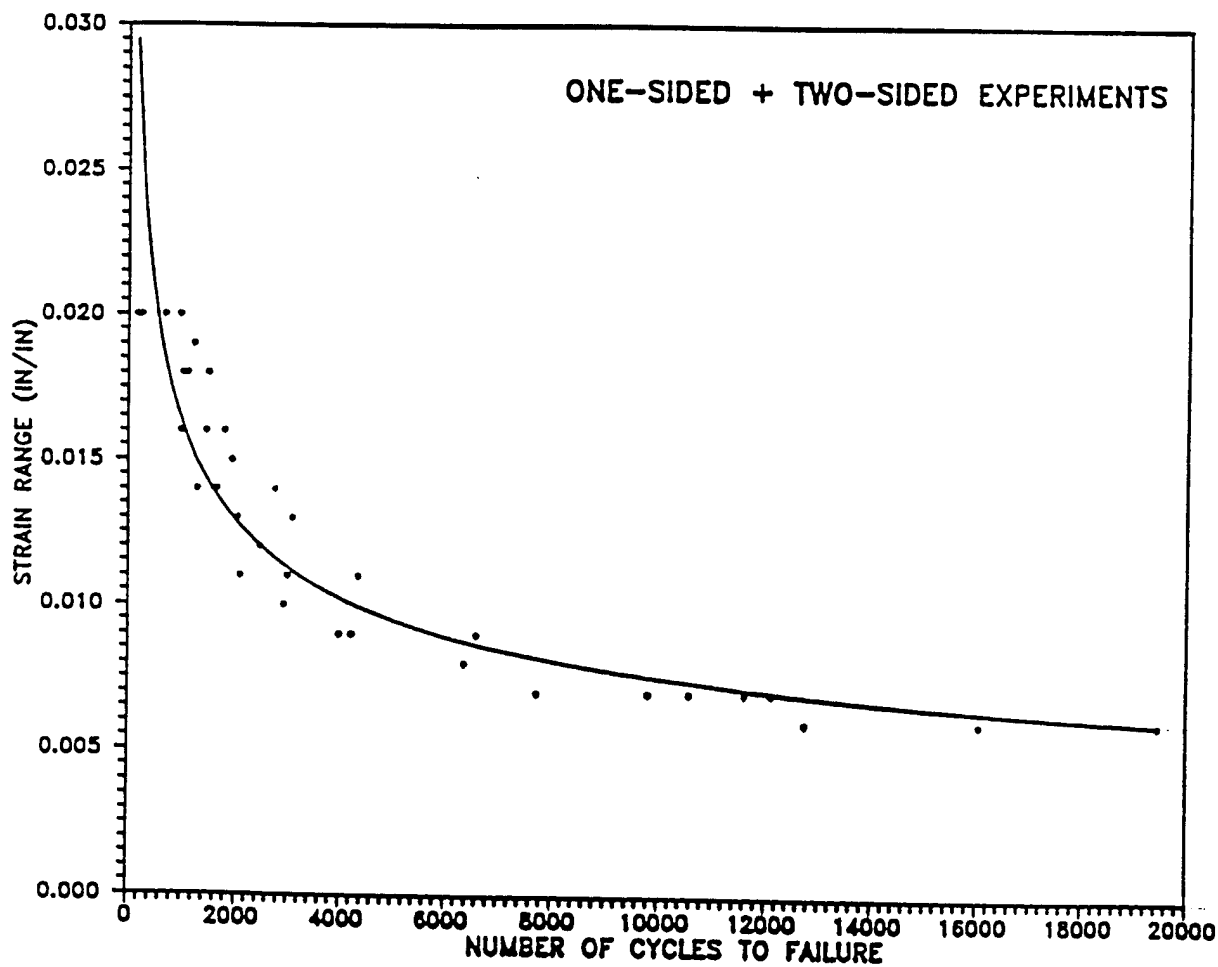
Figure 4.20. Strain Range, $\Delta\epsilon$, versus Number of Cycles to Failure, N_f

$$\langle \Delta U_i \rangle = 90.409 \ N_f^{-0.648} \qquad\qquad r^2 = 0.83 \qquad\qquad (4.8)$$
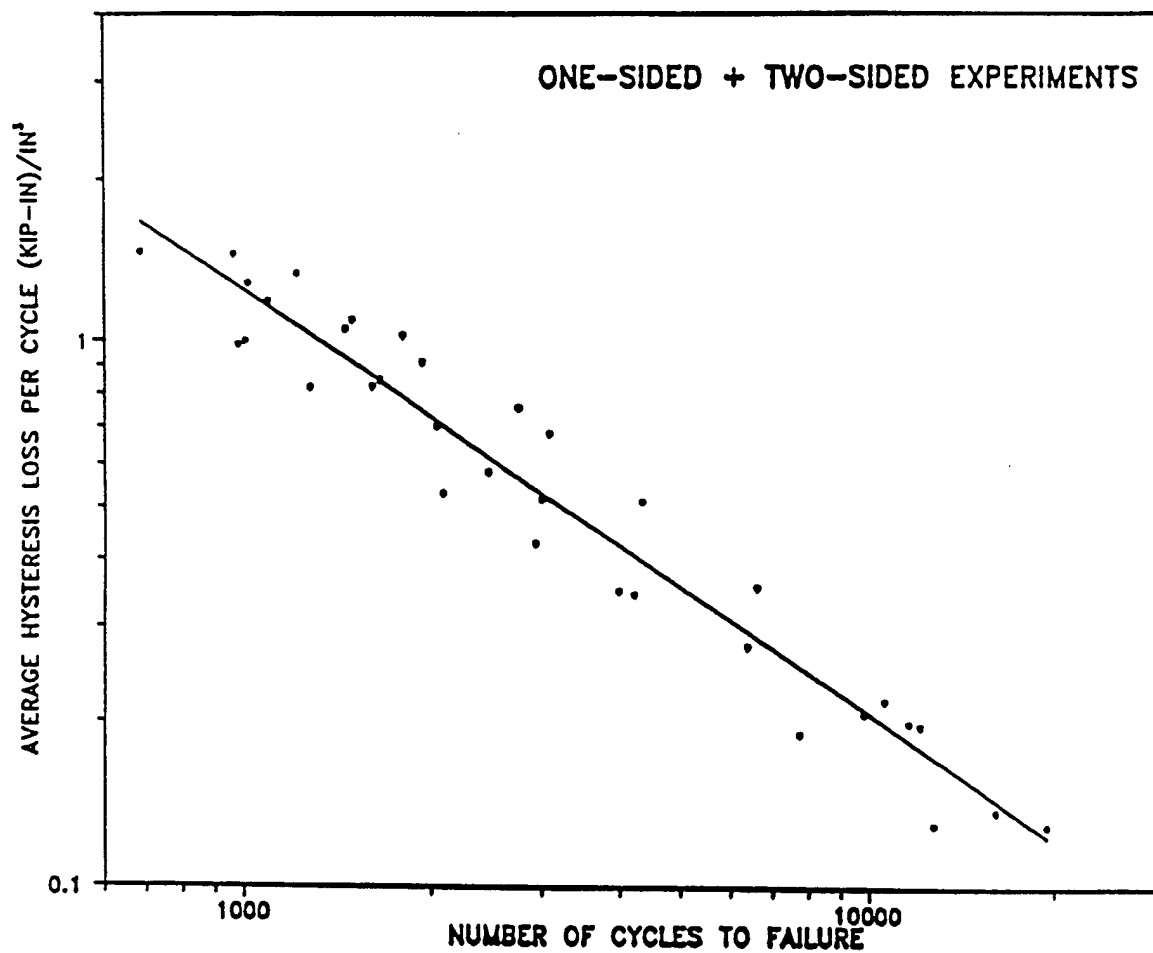
Figure 4.21. Average Hysteresis Loss per Cycle, $\langle \Delta U_i \rangle$,

versus Number of Cycles to Failure, N_f

Similarly, Figure 4.25 displays the N_3 versus N_f data. It may be observed from this figure that the fitted curve represents the data extremely accurately. The equation, which fits this set of data very well, is:

$$N_3 = 0.865 N_f \qquad (4.13)$$

This equation can also be inverted to obtain a means to predict fatigue life as:

$$N_f = 1.157 N_3 \qquad (4.14)$$

In this case, 97% of the data were found to lie within a band whose width is $\pm 5\%$ of the value of N_f predicted by means of Equation 4.13. This equation is conservative for 97% of the data.

Hysteresis Loop Drift Measurement (One-Sided and Two-sided Experiments)

The basic stress-strain data acquired during fatigue experiments can also be used to compute the amount of hysteresis loop displacement in the stress-strain plane. This is defined here as 'loopdrift'. Figure 4.26 defines the concept of the loop drift. This figure combines a graph of maximum stress versus number of cycles and a graph of minimum stress versus number of cycles. The upper, or maximum stress, curve is divided into three regions based on the actual maximum stress encountered in each cycle. The portion of the curve lying between points X and Y represents a region of rapid maximum stress change and the portion of the curve lying between points Y and Z represents a region of moderate or very low maximum stress change.

$$<\Delta U_i> = 92.555 \; \Delta\epsilon - 0.468 \qquad\qquad r^2 = 0.98 \qquad\qquad (4.9)$$
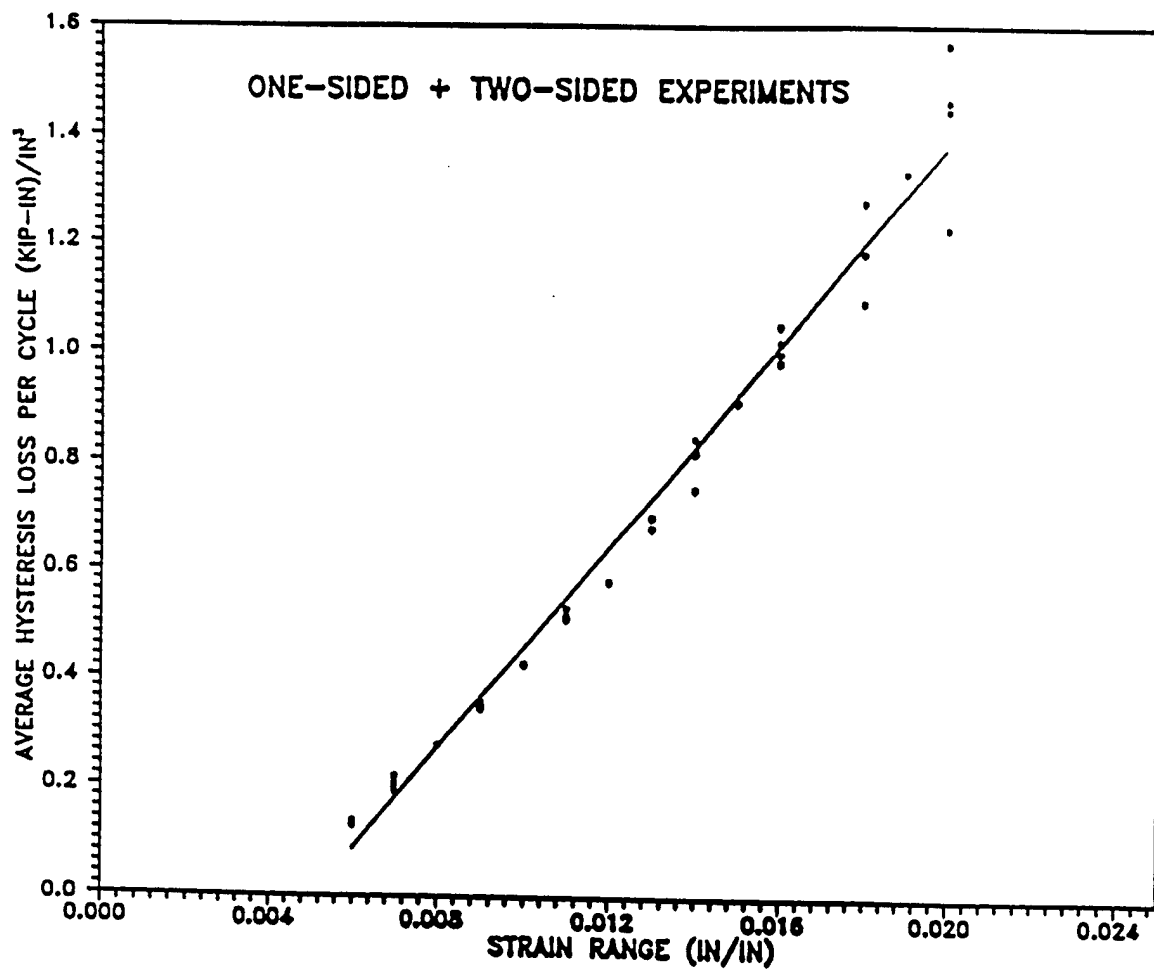
Figure 4.22. Average Hysteresis Loss per Cycle, $<\Delta U_i>$, versus Strain Range, $\Delta\epsilon$

$$\sum \Delta U_i = 95.396 \ N_f^{0.346} \qquad\qquad r^2 = 0.55 \qquad\qquad (4.10)$$
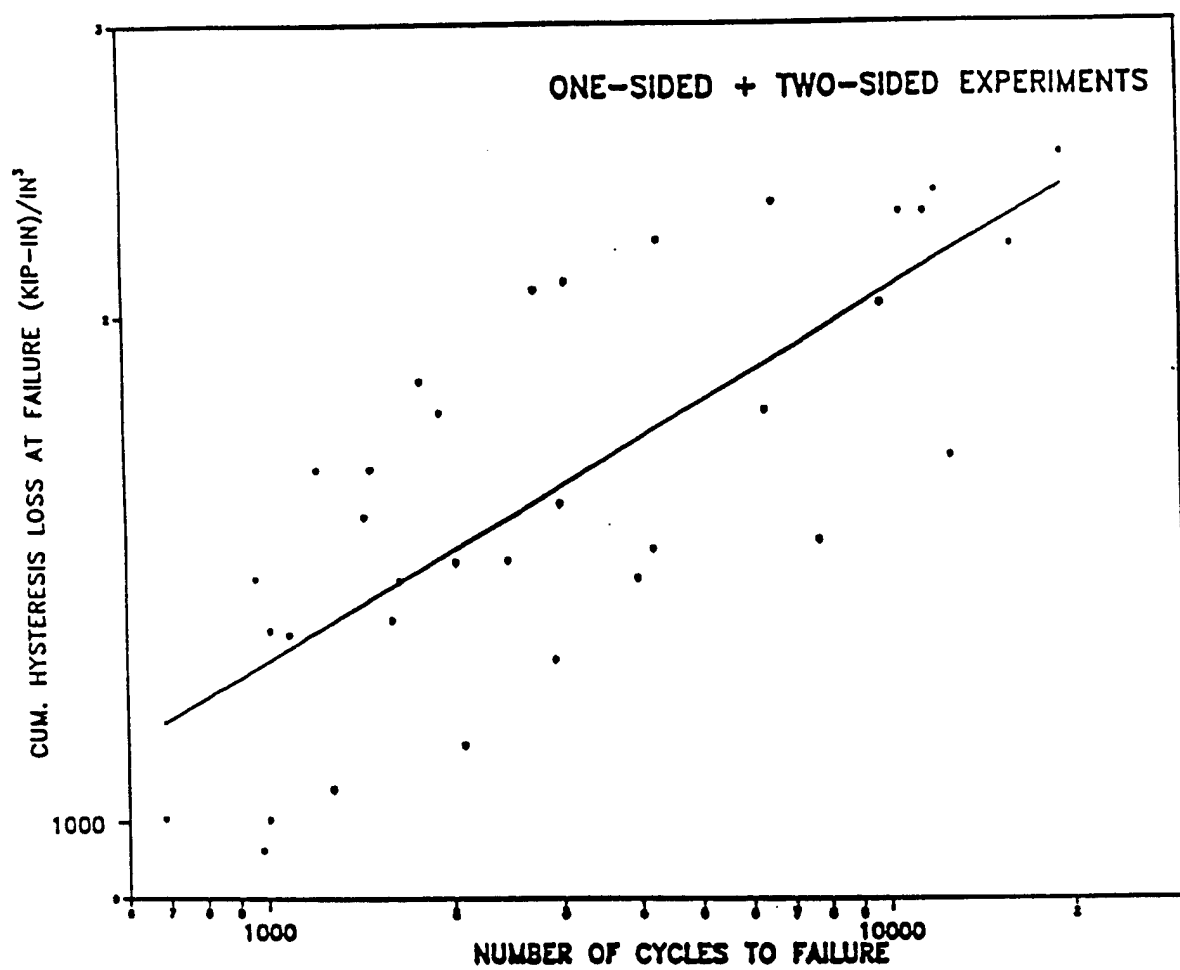
Figure 4.23. Cumulative Hysteresis Loss at Failure, $\sum \Delta U_i$,

versus Number of Cycles to Failure, N_f

Point X occurs at the first cycle, point Y occurs where change in the maximum stress becomes nearly constant and point Z occurs where change in the maximum stress begins to show a significant increase. The following equation defines the drift measure, D1, in ksi:

$$D1 = \left|\sigma_{\max X} - \sigma_{\max Y}\right| + \left|\sigma_{\min X} - \sigma_{\min Y}\right| \qquad (4.15)$$

Hence, D1 is the absolute value of the amount of change in maximum and minimum stresses from point X to point Y. Similarly, the drift measure, D2, is defined as the absolute value of the amount of change in the maximum and minimum stresses from point Y to point Z. That is, D2 in ksi is given by:

$$D2 = \left|\sigma_{\max Y} - \sigma_{\max Z}\right| + \left|\sigma_{\min Y} - \sigma_{\min Z}\right| \qquad (4.16)$$

Using these two definitions, D1 and D2 were computed for all of the 36 experiments conducted in this investigation. Results from the one-sided and two-sided tests are given in Tables A.3 and A.4 of the Appendix A.

Figure 4.27 displays the D1 versus strain range, $\Delta\epsilon$, data. It may be observed from this figure that D1 appears to be only mildly dependent upon the magnitude of the strain range. Similarly, Figure 4.28 which shows the graph of D2 versus strain range, $\Delta\epsilon$, also suggests that D2 may be a constant and does not show appreciable dependence upon the strain range.

$$N_2 = 0.129N_f \qquad\qquad r^2=0.91 \qquad\qquad (4.11)$$
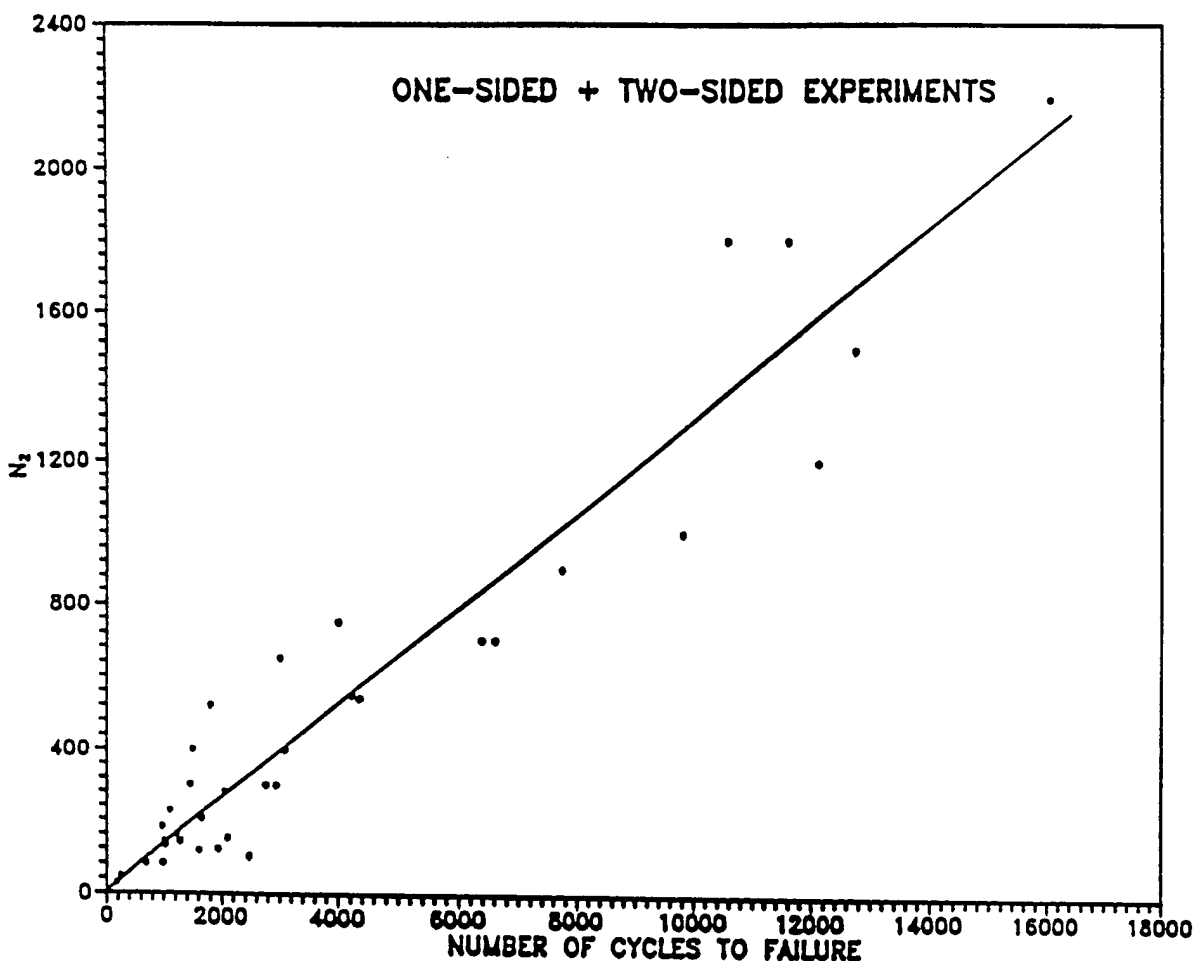
Figure 4.24. N_2 versus Number of Cycles to Failure, N_f

$$N_3 = 0.865 N_f \qquad\qquad r^2 = 0.99 \qquad\qquad (4.13)$$
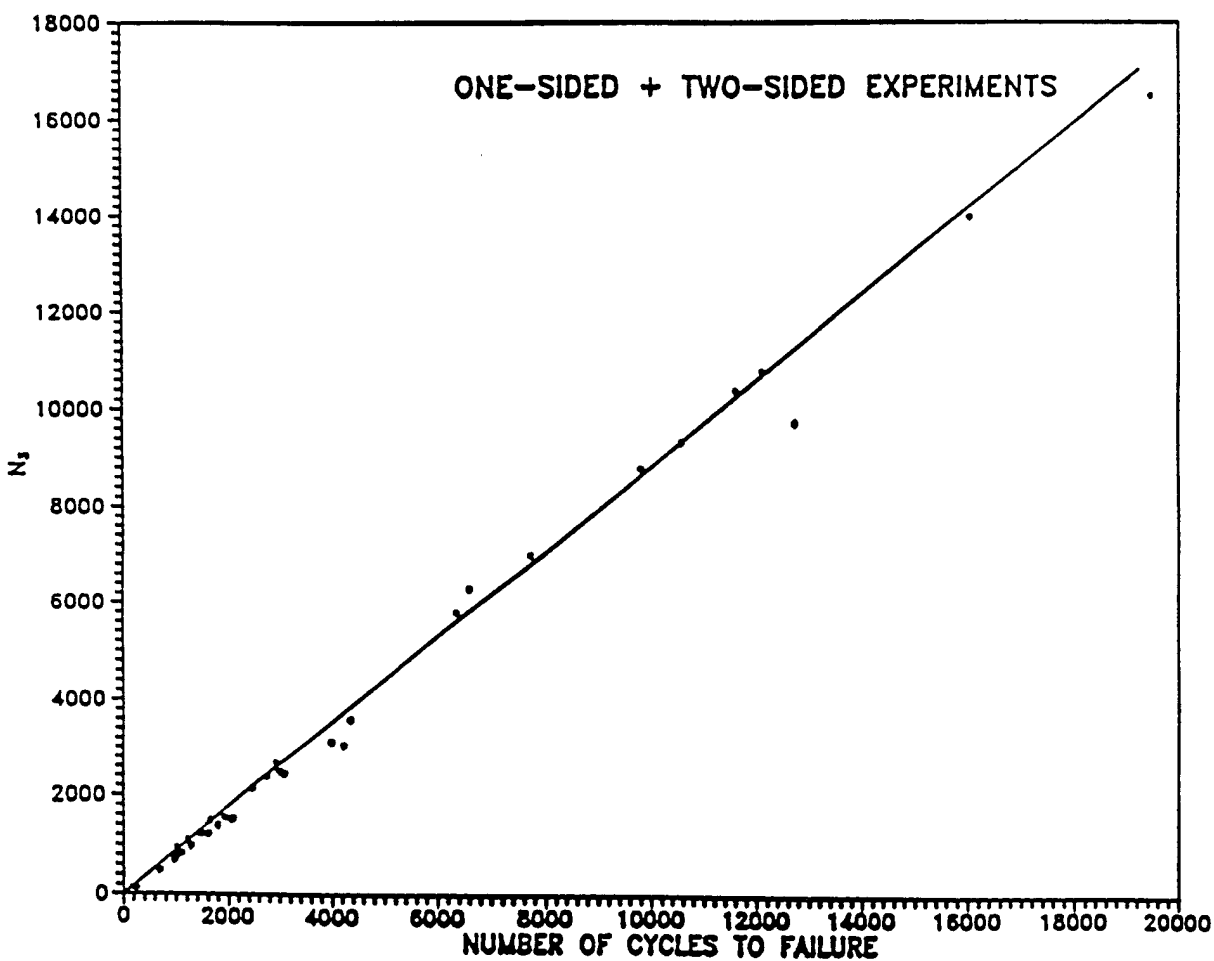
Figure 4.25. N_3 versus Number of Cycles to Failure, N_f

These results suggest that D1 and D2 may be combined into a new measure, D1+D2. Figure 4.29 displays D1+D2 versus strain range data. The results shown in this figure suggest that D1+D2, to a first approximation, may be taken to be a constant. A precise, physical interpretation of these results is not clear at this time. However, it may be possible to correlate the magnitudes of D1, D2 and D1+D2 with fatigue damage for the reason that they appear to be constants. Hence, they may indeed be intrinsic properties of the specimen material.
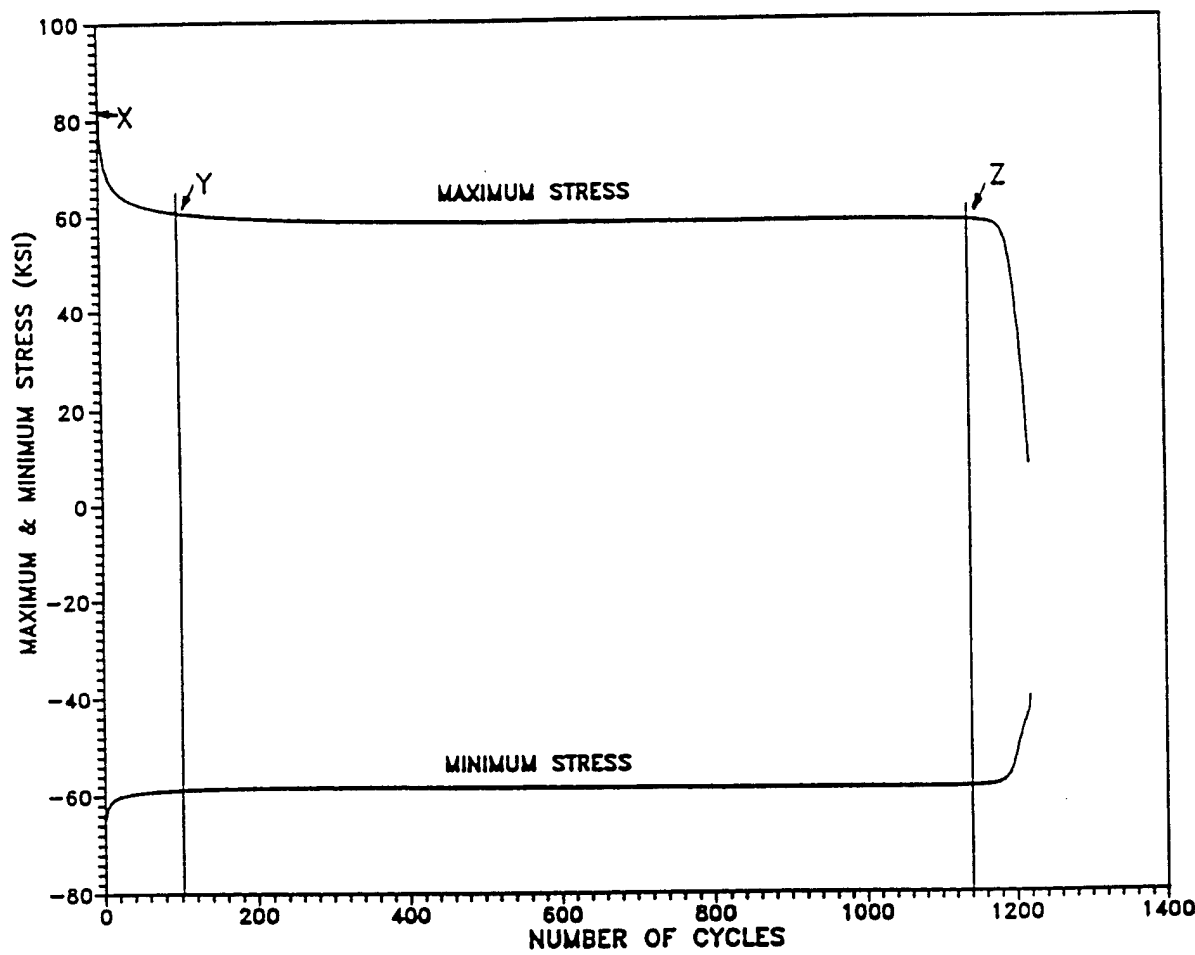
Figure 4.26. Definition of D1 and D2
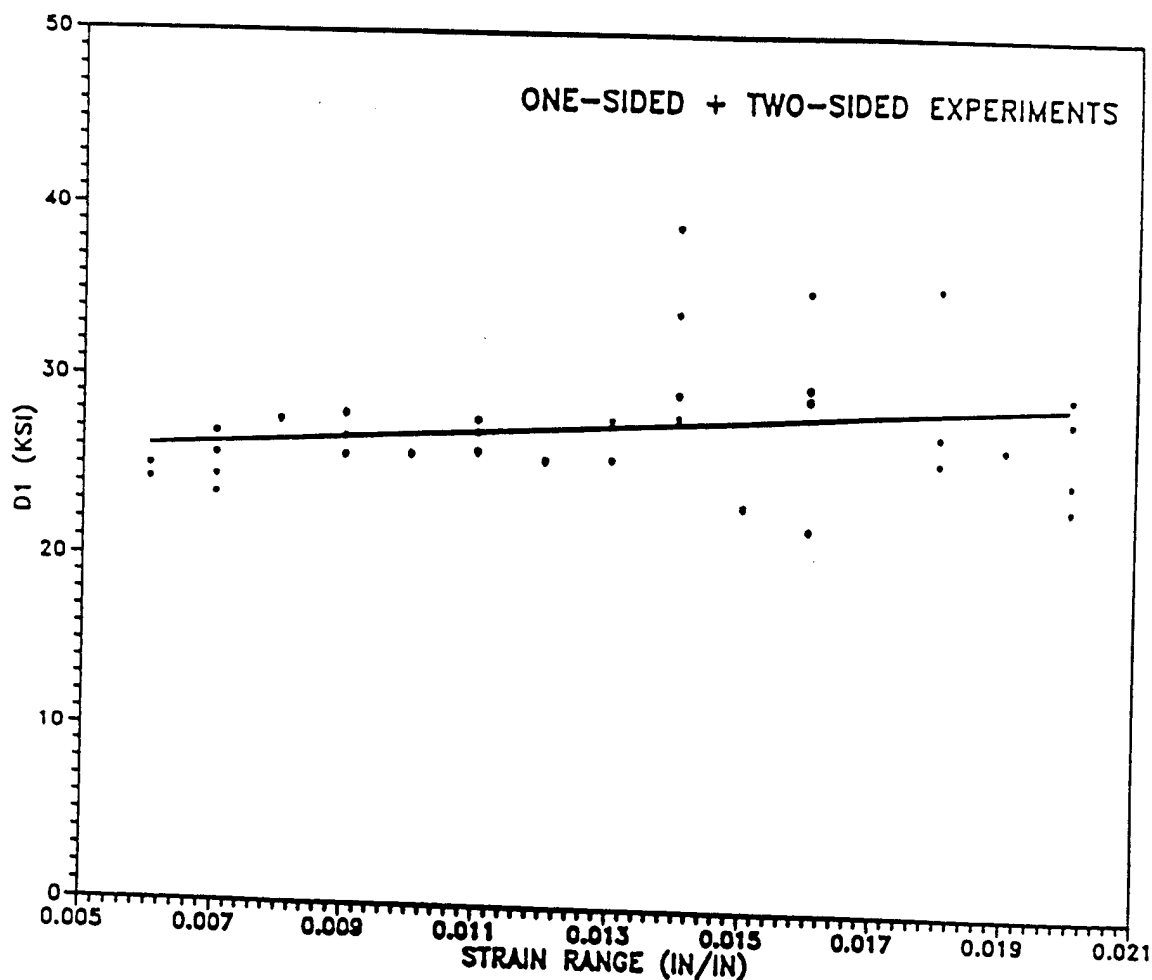
Figure 4.27. Drift, D1, versus Strain Range, $\Delta\epsilon$
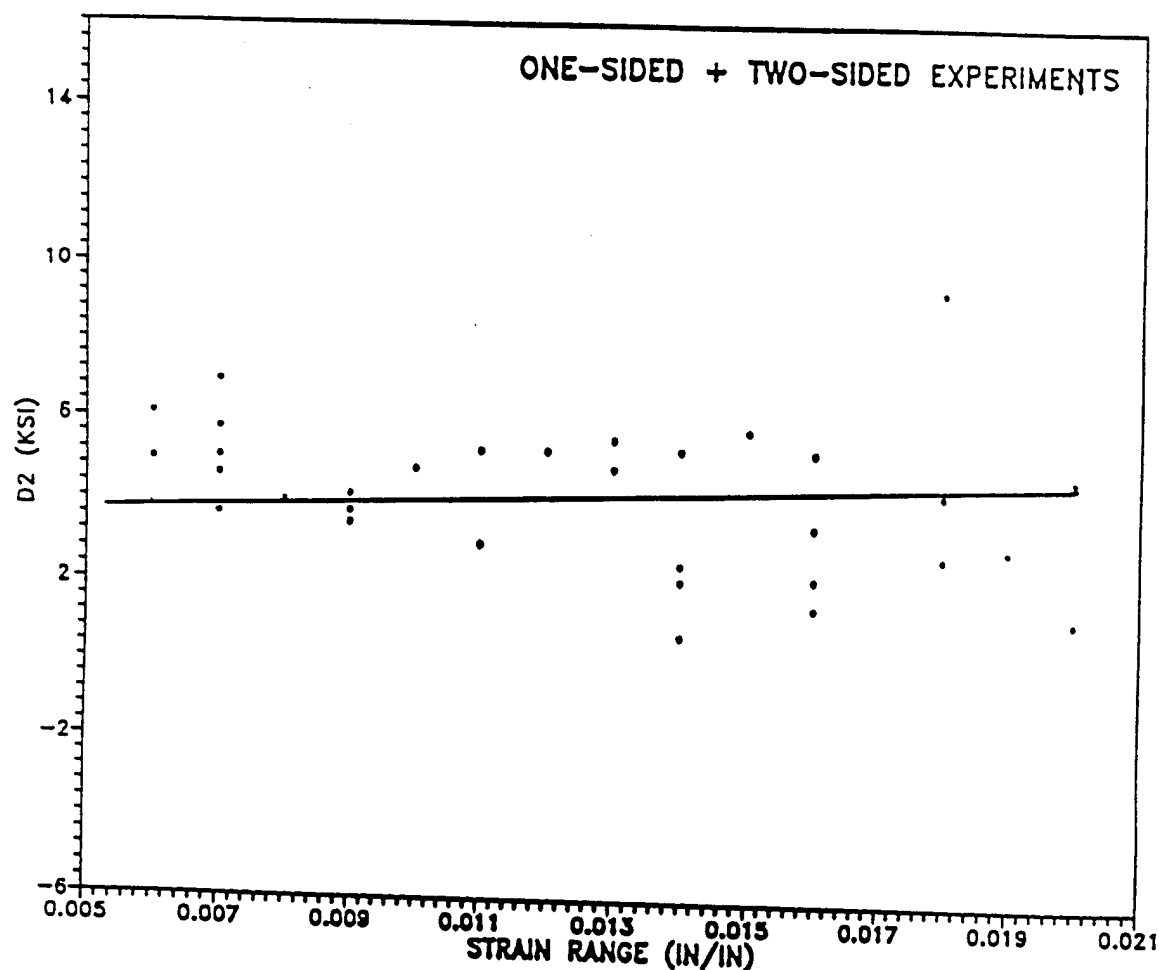
Figure 4.28. Drift, D2, versus Strain Range, $\Delta\epsilon$

Figure 4.29. Drift, D1+D2, versus Strain Range, Δε
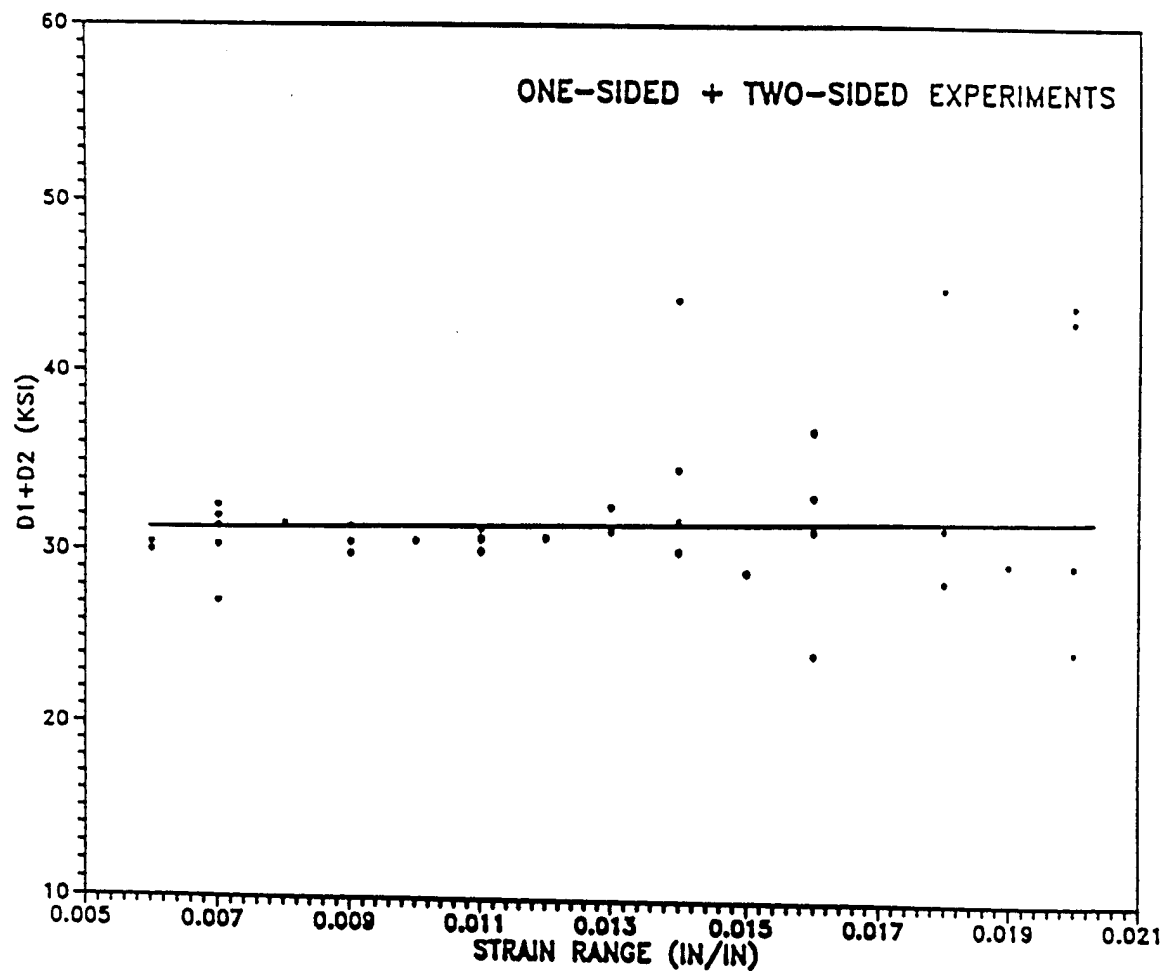
CHAPTER V

CONCLUSIONS

This investigation involved two types of experiments on AISI 1018 unannealed steel specimens. The first set of experiments, the one-sided experiments, involved testing the specimens with non-zero mean strain values and the second set of experiments, the two-sided experiments, were carried out with zero mean strain. All of the tests were of the strain controlled type. The specimens were cycled between pre-set maximum and minimum strain levels and the response of the material was measured in terms of engineering stress values. All of the tests were carried to failure.

Simple, empirical power law equations were derived from the stress-strain measurements to describe the relationships between the average hysteresis loss and the strain range, and the average hysteresis loss and the number of cycles to failure. As was explained earlier, these relationships can be used very effectively to estimate the endurance limit of the material using considerably less effort than is needed with conventional strain-life or stress-life methods. The relationships between N_2 and N_f and N_3 and N_f appear to provide very simple, but reasonably reliable, fatigue failure prediction methods. The preliminary results from the hysteresis loop drift measurements show that this method of analysis is a promosing one and deserves further exploration. Hysteresis loop drift measurements may prove to be extremely useful in connection with materials which do not exhibit well-defined hysteresis loops. Preliminary experiments on 2024-T351 and 7075-T651 aluminium specimens have shown that tests conducted at strain ranges smaller than 0.010

in/in do not display hysteresis loops wide enough to determine the hysteresis loop area. In such cases, hysteresis loop drift measurements may be the only useful approach to carry out a macroscopic analysis of the test results.

The methods of analysis developed in this investigation may be enhanced by means of the following improvements. The experiments in this investigation were conducted using strain ranges which were confined to a band between 0.006 in/in and 0.020 in/in. To estimate the endurance limit more precisely, experiments conducted at smaller strain ranges should be added to the set of experiments reported herein. Also, all of the experiments conducted during this investigation were constrained to a constant preset strain limits. Hence, the effects of cycles of overstrain, if any, is unknown. The method to determine the points N_2 and N_3 needs further refinement. It may be possible to develop a better algorithm to identify these two points without recourse to purely manual methods. This will improve accuracy and may, therefore, further improve fatigue failure predictions. A better correlation of hysteresis loop drift with respect to cumulative fatigue damage needs to be established. This investigation did not explore the implications of the results with respect to actual engineering practice. Such application to actual design practice may prove to be a very significant research contribution in its own right. Finally, combining the macroscopic measurements presented in this investigation with microscopic measurements obtained by means of Acoustic Emission and Magnetic Filed measurements may lead to valuable and original insights regarding the actual origin and inception of the fatigue process in metals.

APPENDIX A

TABULATION OF TEST RESULTS

Table A.1. One Sided Tests Carried To Failure, Hysteresis Loss Results (R = 0)*

Specimen Number	Strain Range, in/in	Cycles to Failure, N_f	Cumulative Hysteresis Loss, (kip-in)/in^3	Average Hysteresis Loss per Cycle, (kip-in)/in^3	N_2	N_3
529	0.020	172	269.37	1.566	28	128
528	0.020	247	341.18	1.387	45	120
221N	0.019	1219	1624.11	1.332	160	1100
530	0.018	1489	1624.23	1.091	400	1240
533	0.016	1005	1002.95	0.998	140	760
331N	0.016	980	961.95	0.982	80	760
334N	0.015	1930	1753.60	0.909	120	1560
531	0.014	1278	1044.98	0.818	140	980
532	0.014	2752	2072.02	0.753	300	2400
113N	0.012	2467	1430.90	0.580	100	2150
335N	0.011	4350	2222.03	0.511	540	3600
116N	0.010	2929	1247.48	0.426	300	2680
119N	0.009	6603	2347.02	0.355	700	6300
121N	0.008	6375	1757.70	0.276	700	5800
228N	0.007	7739	1470.27	0.190	900	7000
220N	0.007	9812	2028.92	0.207	1000	8800
114N	0.007	12112	2381.52	0.197	1200	10800
330N	0.006	19460	2509.09	0.129	1000	16500

* Refer to Figure 3.6 for an explanation of the one-sided test

Table A.2. Two Sided Tests Carried To Failure, Hysteresis Loss Results (R = -1)*

Specimen Number	Strain Range, in/in	Cycles to Failure, N_f	Cumulative Hysteresis Loss, (kip-in)/in^3	Average Hysteresis Loss per Cycle, (kip-in)/in^3	N_2	N_3
118N	0.014	1650	1391.53	0.843	205	1495
115N	0.014	1604	1317.72	0.822	115	1220
110N	0.007	11609	2308.99	0.199	1800	10400
111N	0.007	10582	2310.50	0.218	1800	9350
222N	0.006	12741	1649.86	0.130	1500	9750
223N	0.006	16056	2200.36	0.137	2200	14000
224N	0.013	3085	2095.09	0.679	400	2450
225N	0.013	2038	1426.63	0.700	280	1525
227N	0.009	4224	1452.72	0.344	550	3050
229N	0.009	3992	1394.90	0.349	750	3125
230N	0.011	2999	1548.79	0.516	650	2500
231N	0.011	2090	1107.51	0.529	150	1525
232N	0.016	1451	1523.14	1.049	300	1245
233N	0.016	1796	1830.93	1.020	520	1390
234N	0.018	1094	1291.53	1.181	225	840
332N	0.018	1018	1298.95	1.276	130	940
333N	0.020	965	1395.40	1.446	180	695
336N	0.020	687	1004.16	1.462	80	490

* Refer to Figure 3.7 for an explanation of the two-sided test

Table A.3. One Sided Tests Carried To Failure, Loop Drift Results (R = 0)*

Specimen Number	Strain Range, in/in	Cycles to Failure, N_f	D1, ksi	D2, ksi	D1+D2, ksi
529	0.020	172	28.064	15.079	43.143
528	0.020	247	29.409	14.642	44.051
221N	0.019	1219	26.579	2.045	29.524
530	0.018	1489	35.684	9.355	45.039
533	0.016	1005	35.407	1.460	36.867
331N	0.016	980	22.044	5.252	24.296
334N	0.015	1930	23.237	5.770	29.007
531	0.014	1278	34.031	0.705	34.736
532	0.014	2752	39.078	5.289	44.367
113N	0.012	2467	25.578	5.250	30.828
335N	0.011	4350	26.022	5.242	31.314
116N	0.010	2929	25.824	4.775	30.599
119N	0.009	6603	28.012	3.461	31.473
121N	0.008	6375	27.614	3.980	31.594
228N	0.007	7739	23.515	3.662	27.177
220N	0.007	9812	25.075	4.616	30.321
114N	0.007	12112	24.511	6.923	31.434
330N	0.006	19460	---------	-------	--------

Table A.4. Two Sided Tests Carried To Failure, Loop Drift Results (R = -1)*

Specimen Number	Strain Range, in/in	Cycles to Failure, N_f	D1, ksi	D2, ksi	D1+D2, ksi
118N	0.014	1650	28.013	2.109	30.122
115N	0.014	1604	29.325	2.507	31.832
110N	0.007	11609	26.897	5.055	31.952
111N	0.007	10582	26.837	5.751	32.588
222N	0.006	12741	24.313	6.087	30.400
223N	0.006	16056	25.028	4.974	30.002
224N	0.013	3085	25.704	5.531	31.235
225N	0.013	2038	27.813	4.814	32.627
227N	0.009	4224	25.743	4.139	29.882
229N	0.009	3992	26.778	3.741	30.519
230N	0.011	2999	27.734	2.984	30.718
231N	0.011	2090	27.097	2.945	30.042
232N	0.016	1451	29.126	2.188	31.314
233N	0.016	1796	29.763	3.461	33.224
234N	0.018	1094	27.177	4.257	31.434
332N	0.018	1018	25.784	2.745	28.529
333N	0.020	965	24.788	4.656	29.444
336N	0.020	687	23.357	1.193	24.550

BIBLIOGRAPHY

American Institute of Steel Construction (1989), Manual of Steel Construction, Allowable Stress Design, 9th ed., AISC, Chicago, Illinois, pp. 5 - 202, 1989.

Albert (1896), Stahl u. Eisen, 1896, pp. 437.

American Society for Metals (I - 1986), Atlas of Fatigue Curves, 2nd printing, Carnes Publishing Services Inc., May, 1986, pp. 43.

American Society for Metals (II - 1986), Metals Handbook, 9th ed., Vol. 1, Carnes Publishing Services Inc., 1986, pp. 125, 223, 241.

Bannantine, J., Comer, J. and Handrock, J. (1990), Fundamentals of Metal Fatigue Analysis, Prentice Hall, New Jersey, 1990.

Basquin, O. (1910), "The Exponential Law of Endurance Tests", Proceedings of the American Society for Testing and Materials, Vol. 10, 1910, pp. 625 - 630.

Coffin, L. and Tavernelli, J. (1959), "The Cyclic Straining and Fatigue of Metals", Transactions of the Metallurgical Society, American Institute for Mining Engineering, Vol. 215, Oct., 1959, pp. 794 - 806.

Cohn, M., Ghosh, S., and Parimi, S. (1972), "Unified Approach to Theory of Plastic Structures", Journal of the Engineering Mechanics Division, Proceedings of the American Society of Civil Engineers, Vol. 98, No. EM5, Oct., 1972, pp. 1133 - 1157.

Ewing, Sir J. and Rosenhain, W. (1899), "Experiments in Micro-Metallurgy - Effects of Strain", Proceedings of the Royal Society of London, Vol. 65, 1899, pp. 85.

Ewing, Sir J. and Humphrey, J. (1903), "Fracture of Metals Under Repeated Alternations of Stress", Philosophical Transactions of the Royal Society of London, Vol. 200a, 1903, pp. 241.

Feltner, C. and Morrow, J. (1961), "Microplastic Strain Hysteresis Energy as a Criterion for Fatigue Fracture", Journal of Basic Engineering, Series D, Transactions of the American Society of Mechanical Engineers, Vol. 83, March 1961, pp. 15 - 22.

French, H. (1933), "Fatigue and the Hardening of Steels", Transactions of the ASST, Oct., 1933, pp. 899 - 946.

Gerber, W. (1874), "Relation Between the Superior and Inferior Stresses of a Cycle of Limiting Stress", Zeit. Bayerischen Arch. Ing.- Vereins, 1874.

Goodman, J. (1899), Mechanics Applied to Engineering, Longmans, Green and Co., London, England, 1899.

Guralnick, S. (1973), "Incremental Collapse Under Conditions of Partial Unloading", International Association for Bridge and Structural Engineering, Vol. 33 Part II, 1973.

Guralnick, S. (1975), "An Incremental Collapse Model for Metal Fatigue", International Association for Bridge and Structural Engineering, Vol. 35 Part II, 1975, pp. 634 - 650.

Guralnick, S., Singh, S. and Erber, T. (1984), "Plastic Collapse, Shakedown and Hysteresis", Journal of Structural Engineering, Vol. 110, No. 9, Sept., 1984, pp. 2103 - 2119.

Guralnick, S., Erber, T., Stefanis, J., and Soudan, O. (1986), "Plastic Collapse, Shakedown and Hysteresis of Multistory Steel Structures", Journal of Structural Engineering, Vol. 112, No. 12, Dec., 1986, pp. 2610 - 2627.

Guralnick, S., Erber, T., Soudan, O. and Stefanis, J. (1988), "Energy Method for Incremental Collapse Analysis of Framed Structures", Journal of Structural Engineering, Vol. 114, No. 1, Jan., 1988, pp. 31 - 49.

Guralnick, S. and Erber, T. (1990), The Hysteresis and Incremental Collapse of Complex Structures: A Paradigm for the Fatigue Failure of Materials, Annual Report submitted to Air Force Office of Scientific Research (grant no. 2302/B2) by the Civil Engineering Department of the Illinois Institute of Technology, Chicago, Illinois.

Guralnick, S. and Erber, T. (1992), Fatigue, Hysteresis and Acoustic Emission, Final Report submitted to Air Force Office of Scientific Research (grant no. AFOSR-91013 DEF, ORAA NO. A0103-1-29110) by the Civil Engineering Department of the Illinois Institute of Technology, Chicago, Illinois.

Halford, G. and Morrow, J. (1962), "Low Cycle Fatigue in Torsion", Proceedings of the American Society for Testing and Materials, Vol. 62, 1962, pp. 695 - 707.

Halford, G. (1963), "The Strain Hardening Exponent - A New Interpretation and Definition", Transactions Quarterly, American Society for Metals, Vol. 56, No. 3, Sept., 1963, pp. 787 - 788.

Halford, G. (1966), "The Energy Required for Fatigue", Journal of Materials, Vol. 1, No. 1, March, pp. 3 - 18.

He, J. (1990), The Hysteresis and Incremental Collapse of Multi-Bay, Multi-Story Framed Structures, thesis, presented to the Illinois Institute of Technology, Chicago, Illinois, in partial fulfillment of the requirements for the degree of Doctor of Philosophy, Aug., 1990.

Johnson, J. (1922), Materials of Construction, 5th ed., 1922.

Landgraf, R. (1970), "The Resistance of Metals to Cyclic Deformation", In Achievement of High Fatigue Resistance in Metals and Alloys, ASTM STP 467, American Society for Testing and Materials, 1970, pp. 3 - 35.

Launhardt (1873), "Formula for Range of Stress", Zeit. Arch. Ing. Vereins, Hanover, 1873.

Martin, D. (1961), "An Energy Criterion for Law Cycle Fatigue", Journal of Basic Engineering, Series D, Transactions of the American Society of Mechanical Engineers, Dec., 1961, pp. 565 - 571.

Michels, S. (1991), Hysteresis and Fatigue, thesis, presented to The Illinois Institute of Technology, Chicago, Illinois, in partial fulfillment of the requirements for the degree of Master of Science, Aug., 1991.

Miner, M. (1945), "Cumulative Damage in Fatigue", Transactions of the American Society of Mechanical Engineers, Vol. 67, Sept., 1945, pp. A159 - A164.

Mitchell, M. (1978), "Fundamentals of Modern Fatigue Analysis for Design",In Fatigue and Micro-Structures, papers presented at the 1978 ASM Materials Science Seminar, American Society for Metals, 1978, pp. 385 - 437.

Moore, H. and Kommers, J. (1927), The Fatigue of Metals, McGraw-Hill Book Co., Inc., NY, NY, 1927.

Morrow, J. (1964), "Cyclic Plastic Strain Energy and Fatigue of Metals", In Internal Friction, Damping and Cyclic Plasticity, ASTM STP 378, American Society for Testing and Materials, 1964, pp. 45 - 87.

Nadai, A. (1931), Plasticity, 5th impression, McGraw-Hill Book Co., Inc., NY, NY, 1931.

Neal, B. (1956), The Plastic Methods of Structural Analysis, Chapman and Hall, London, England, 1956.

Popov, E., and McCarthy, R. (1960), "Deflection Stability of Frames Under Repeated Loads", Journal of Engineering Mechanics Division, Proceedings of the American Society of Civil Engineers, Vol. 86, No. EM1, Jan., 1960, pp. 61 - 79.

Popov, E. and Bertero, V. (1973), "Cyclic Loading of Steel Beams and Connections", Journal of the Structural Division, Proceedings of the American Society of Civil Engineers, Vol. 99, No. ST6, June, 1973, pp. 1189 - 1204.

Popov, E. and Peterson, H. (1978), "Cyclic Metal Plasticity: Experiments and Theory", Journal of the Engineering Mechanics Division, Proceedings of the American Society of Civil Engineers, Vol. 104, No. EM6, Dec., 1978, pp. 1370 - 1387.

Sih, G. (1985), "Mechanics and Physics of Energy Density Theory", Theoretical and Applied Fracture Mechanics, No. 4, 1985, pp. 157 - 173.

Symonds, P. (1952), Discussion of "Welded Continuous Frames: Plastic Design and the Deformation of Structures", Welding Journal, 1952, pp. 33-s - 36-s.

Weyrauch, J. (1880-81), "On the Calculations of Dimensions as Depending on the Ultimate Working Strength of Materials", Proceedings of the British Institute of Civil Engineering, Vol. 63, 1880-81, pp. 275.

Wöhler, A. (1860-71), Zeit. fur Bauwesen, Vols. 10, 13, 16, 20, 1860-71.

REPORT DOCUMENTATION PAGE

Public reporting burden for this collection of information is estimated to average 1 hour per response, including the time for reviewing instructions, searching existing data sources, gathering and maintaining the data needed, and completing and reviewing the collection of information. Send comments regarding this burden estimate or any other aspect of this collection of information, including suggestions for reducing this burden, to Washington Headquarters Services, Directorate for Information Operations and Reports, 1215 Jefferson Davis Highway, Suite 1204, Arlington, VA 22202-4302, and to the Office of Management and Budget, Paperwork Reduction Project (0704-0188), Washington, DC 20503.

1. AGENCY USE ONLY (Leave blank)	2. REPORT DATE	3. REPORT TYPE AND DATES COVERED
		FINAL REPORT 1 Mar 93 - 31 Mar 95

4. TITLE AND SUBTITLE	5. FUNDING NUMBERS
Hysteresis and Acoustic Emission as Non-Destructive Measures of the Fatigue Process in Metals	61102F 2300/HS

6. AUTHOR(S)

Professor Guralnick

7. PERFORMING ORGANIZATION NAME(S) AND ADDRESS(ES)	8. PERFORMING ORGANIZATION REPORT NUMBER
Illinois Institute of Technology IIT Center Chicago, IL 60616	AFOSR-IR 95-0464

9. SPONSORING/MONITORING AGENCY NAME(S) AND ADDRESS(ES)	10. SPONSORING/MONITORING AGENCY REPORT NUMBER
AFOSR/NE 110 Duncan Avenue Suite B115 Bolling AFB DC 20332-0001	F49620-93-1-0157

11. SUPPLEMENTARY NOTES

12a. DISTRIBUTION/AVAILABILITY STATEMENT

APPROVED FOR PUBLIC RELEASE: DISTRIBUTION UNLIMITED

12b. DISTRIBUTION CODE

13. ABSTRACT (Maximum 200 words)

SEE FINAL REPORT ABSTRACT

DTIC SELECTED
JUN 2 8 1995
F
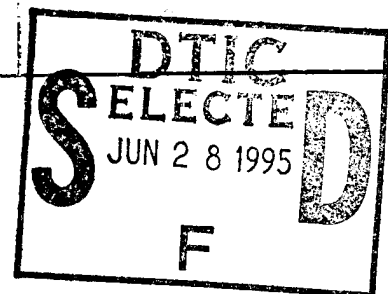
DTIC QUALITY INSPECTED 1

14. SUBJECT TERMS

	15. NUMBER OF PAGES
	16. PRICE CODE

17. SECURITY CLASSIFICATION OF REPORT	18. SECURITY CLASSIFICATION OF THIS PAGE	19. SECURITY CLASSIFICATION OF ABSTRACT	20. LIMITATION OF ABSTRACT
UNCLASSIFIED	UNCLASSIFIED	UNCLASSIFIED	UNCLASSIFIED